Imaging and characterization of solute transport during two tracer tests in a shallow aquifer using electrical resistivity tomography and multilevel groundwater samplers

Kerstin Müller,[1,2] Jan Vanderborght,[1] Andreas Englert,[1,3] Andreas Kemna,[1,4] Johan A. Huisman,[1] Joerg Rings,[1] and Harry Vereecken[1]

Received 18 November 2008; revised 25 August 2009; accepted 21 September 2009; published 3 March 2010.

[1] The relevance of aquifer heterogeneity for flow and transport is recognized broadly; however, its characterization is hampered by the inaccessibility of the subsurface. Time-lapse electrical resistivity tomography (ERT) offers the possibility of imaging noninvasively subsurface transport. We present results of two tracer tests that were carried out successively in a shallow aquifer at the Krauthausen test site (Germany). The breakthroughs of an electrically conductive and a resistive tracer were monitored with ERT and local multilevel groundwater samplers (MLS) along two cross sections perpendicular to the mean flow direction. Sinking of the conductive salt tracer due to density effects was observed with ERT. We applied a stream tube model to characterize the spatially variable transport. ERT-derived stream tube parameters showed similar patterns for the two tracer experiments, reflecting the effect of aquifer heterogeneity on transport. MLS data did not show similar spatial patterns, which indicates that these measurements may be prone to subtle changes of the flow field in the small sampling volume and mixing within screened wells. Between 50% and 10% of the tracer was recovered in the ERT-derived breakthrough curves. Compared with transport simulations in a homogeneous aquifer, ERT-derived time-integrated changes in electrical conductivity were locally larger but focused in a smaller area. MLS data indicated that in this area, ERT did not underestimate the tracer recovery. The relatively low tracer recovery was attributed to undetected tracer breakthrough in regions with low ERT sensitivity and in regions where the length of the tracer plume and the electrical conductivity contrast were small.

Citation: Müller, K., J. Vanderborght, A. Englert, A. Kemna, J. A. Huisman, J. Rings, and H. Vereecken (2010), Imaging and characterization of solute transport during two tracer tests in a shallow aquifer using electrical resistivity tomography and multilevel groundwater samplers, *Water Resour. Res.*, *46*, W03502, doi:10.1029/2008WR007595.

1. Introduction

[2] Risk assessment of potentially hazardous substances in soils and groundwater requires detailed knowledge about the spatial and temporal variation of transport relevant properties of the subsurface. The use of geophysical methods to characterize the subsurface structure and heterogeneity is documented well in literature since many years. In recent years geophysical methods are increasingly being used to monitor subsurface fluid movement. One geophysical parameter that is sensitive to the change in volumetric water content and ionic strength of the pore water is the bulk electrical conductivity. Monitoring of bulk electrical conductivity may therefore be used to monitor the infiltration of water into the unsaturated zone and/or the displacement of the background pore water by a tracer solution with a different electrical conductivity. Monitoring of bulk electrical conductivities during salt tracer experiments in order to characterize solute transport processes and parameterize transport models has been a common practice in vadose zone hydrology since automated time domain reflectometry (TDR) systems became available [*Kachanoski et al.*, 1992; *Vanclooster et al.*, 1993]. A disadvantage of the TDR technique is that only local bulk soil electrical conductivities are measured and the spatial structures of transport and/or water infiltration are difficult to derive from a set of local measurements.

[3] In order to characterize transport in heterogeneous aquifers, tracer transport is monitored during groundwater tracer tests. Because of the aquifer heterogeneity, such tracer tests require a dense network of groundwater samplers. Because of the high installation costs of a sufficiently dense network of groundwater samplers in combination with the considerable monitoring effort, such experiments were carried out at only a few sites [*Boggs et al.*, 1992; *Hess et al.*, 1992; *Jensen et al.*, 1993; *Leblanc et al.*, 1991; *Sudicky*,

[1]Agrosphere Institute, ICG-4, Forschungszentrum Jülich GmbH, Jülich, Germany.
[2]Now at RWE Dea AG, Hamburg, Germany.
[3]Now at Earth Sciences Department, Ruhr-University Bochum, Bochum, Germany.
[4]Now at Department of Geodynamics and Geophysics, University of Bonn, Bonn, Germany.

0043-1397/10/2008WR007595$09.00

1986; *Vereecken et al.*, 2000]. Similar to the problems with TDR in vadose zone tracer experiments, the density of the local samplers was in several cases insufficient to fully map the concentration distributions. Imaging methods such as electrical resistivity tomography (ERT), which map distributions of electrical conductivity, therefore offer an important advantage compared with local-scale measurements.

[4] ERT has been used to image water infiltration in soils [*Daily et al.*, 1992; *Michot et al.*, 2003; *Park*, 1998; *Zhou et al.*, 2001] and tracer movement in soil columns [*Binley et al.*, 1996; *Köstel et al.*, 2008; *Olsen et al.*, 1999], in soil profiles [*French and Binley*, 2004; *French et al.*, 2002; *Looms et al.*, 2008b], in physical groundwater models [*Slater et al.*, 2002], and in shallow aquifers [*Cassiani et al.*, 2006a; *Kemna et al.*, 2002; *Oldenborger et al.*, 2007; *Singha and Gorelick*, 2005; *Singha et al.*, 2007]. These experiments demonstrated the potential of ERT to image transport processes. But also problems related to sensitivity and spatial resolution of the imaging method, and to the recovered tracer mass were reported. Besides imaging of tracer transport, monitoring of tracer transport using ERT may also be used to parameterize groundwater models. *Binley et al.* [2002], *Deiana et al.* [2007], and *Looms et al.* [2008a] used ERT in combination with ground-penetrating radar data to identify unsaturated hydraulic parameters of a soil and the underlying vadose zone. *Day-Lewis and Singha* [2008] and *Singha et al.* [2008] investigated in numerical experiments and in a pilot-scale case study how mass transfer rates of solutes between mobile and immobile zones could be inferred from ERT measurements. *Vanderborght et al.* [2005] demonstrated in a numerical study how a tracer experiment that is monitored with ERT can be used to derive spatial patterns of stream tube model parameters and how these patterns could be linked to the spatial heterogeneity of the hydraulic conductivity of the aquifer. *Pollock and Cirpka* [2008] presented a perturbation approach to derive the spatial distribution of hydraulic conductivity from time moments of electrical resistance that are measured in ERT surveys. The applicability of this approach was also demonstrated in a numerical experiment. However, the use of ERT surveys for the characterization and quantification of the spatial variability of transport processes has not been demonstrated in many real tracer experiments. *Köstel et al.* [2009a, 2009b] used a stream tube model to characterize the spatial variability of the advection velocity and solute dispersion in an unsaturated soil monolith. By local TDR measurements and tracer concentration measurements in the outflow of the column, they could validate the approach. A similar approach to characterize and quantify transport heterogeneity in an unconfined aquifer based on ERT surveys was followed by *Kemna et al.* [2002]. However, they were not able to validate the obtained results with independent measurements. Second, the scale of the tracer study that was carried out was small, especially when compared with the scale of the aquifer heterogeneities.

[5] The major objective of this study is to compare the quantification of the transport heterogeneity in a shallow aquifer in terms of stream tube parameters that are obtained from ERT surveys along 2-D transects and from surveys of tracer concentrations in multilevel groundwater samplers. Similar to *Kemna et al.* [2002] and *Vanderborght et al.* [2005], we focused on the tracer breakthrough in reference planes that are perpendicular to the mean flow direction instead of using a fully 3-D characterization of the tracer plume. By focusing on reference planes, ERT data acquisition time and the number of boreholes that is needed to image the transport process can be reduced while maintaining a sufficiently high spatial resolution to visualize the effects of aquifer heterogeneity on transport.

[6] As in the work by *Kemna et al.* [2002], the Krauthausen test site was used. However, larger tracer volumes were injected in the aquifer than in the test carried out by *Kemna et al.* [2002] in order to investigate the transport process in a larger volume of the aquifer and visualize the effect of aquifer heterogeneity on transport. Therefore, in the current study, tracer was injected over an 8 m thick section of the aquifer and monitored over a distance of 20 m downstream from the injection well as compared to a 1 m thick injection and 5 m downstream monitoring in the work by *Kemna et al.* [2002].

[7] A second set of objectives was to test the reproducibility of tracer tests and to evaluate the effect of density driven flow on tracer transport and the characterization of tracer transport in a heterogeneous aquifer. Therefore two tracer tests were carried out under similar boundary conditions: one using a salt tracer with a higher electrical conductivity than the groundwater and one with a "negative" tracer with a lower electrical conductivity.

2. Material and Methods

2.1. Description of Test Site and Tracer Tests

[8] The Krauthausen test site is situated approximately 10 km northwest of the city of Düren and 6 km southeast of the Forschungszentrum Jülich GmbH, Germany. A detailed description of the Krauthausen test site is given by *Döring* [1997], *Englert* [2003], and *Vereecken et al.* [2000]. The field has an extent of 60 m by 200 m. The upper aquifer system is composed of unconsolidated Quaternary deposits, and a silty soil at the top. The base of the aquifer consists of thin layers of clay and silt and is situated between 11 m and 13 m below the surface. The geometric mean and variance of the log transformed hydraulic conductivity of the aquifer are estimated to be 0.0013 m s^{-1} and 1.3, respectively, and the spatial correlation in the horizontal and vertical direction is 6.7 m and 0.37 m, respectively [*Döring*, 1997]. The porosity is 26% with a standard deviation of 6% [*Vereecken et al.*, 2000]. The main direction of the groundwater flow is toward NW with a hydraulic gradient of about 0.002, which stays fairly constant over time. The groundwater table shows significant seasonal variation ranging from 2.5 m to 1 m below surface in summer and winter, respectively.

[9] The test site comprises 76 observation wells reaching to a depth of 10–11 m below the surface. The drilling diameter for all wells was 328 mm in which screened PVC tubes with a diameter of 50 mm were installed. Most of the wells are screened between 3 m and 10 m below the surface. Sixty six of the 76 observation wells are equipped with multilevel groundwater samplers (MLS). These consist of a bundle of 24 polyethylene tubes (outer diameter 5 mm) of different length attached to the outside wall of an observation well allowing a depth dependent sampling over 0.3 or 0.35 m intervals. The locations of the observation wells at the test site are shown in Figure 1.

[10] Two large-scale tracer experiments were carried out consecutively at the test site from September until December

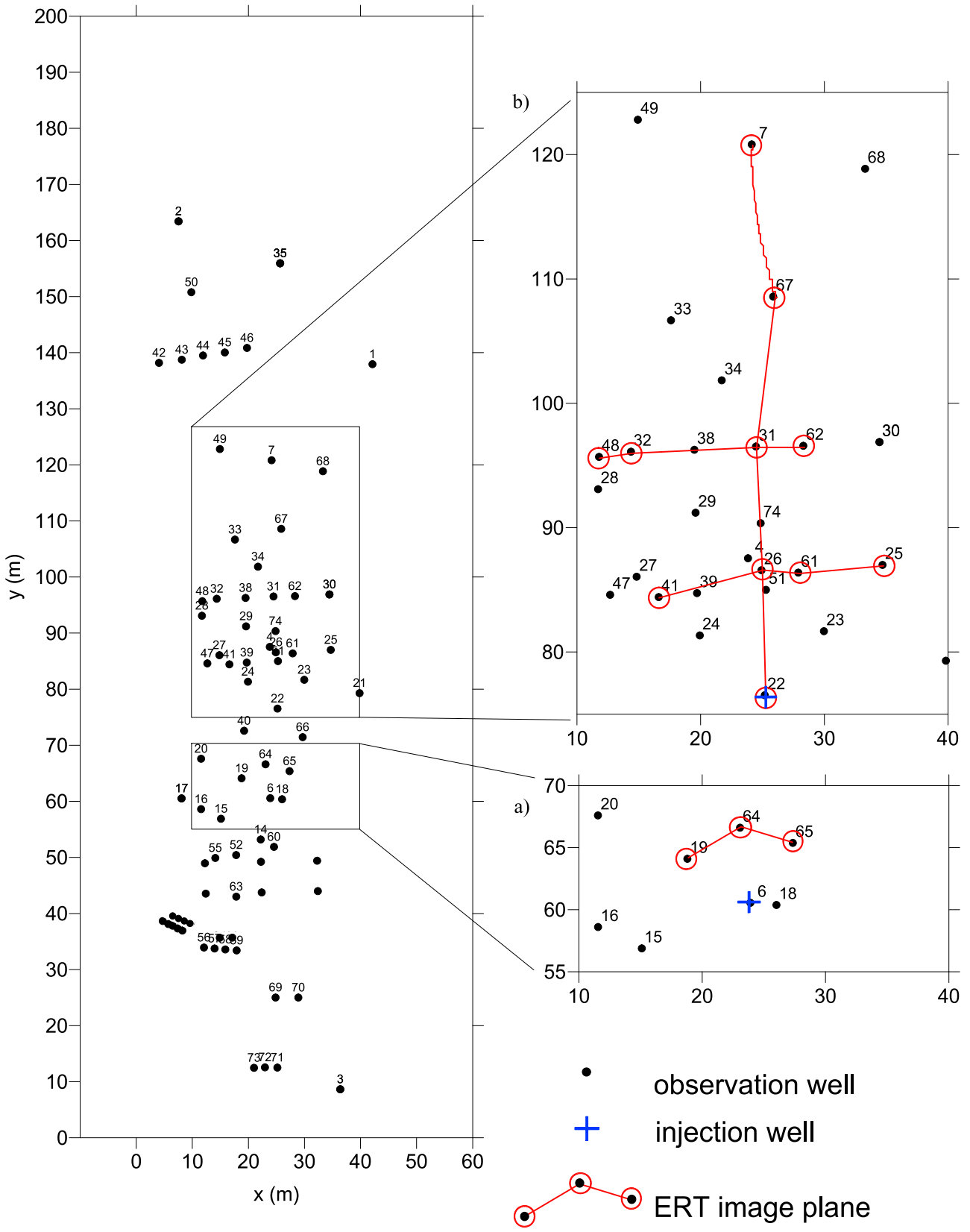

Figure 1. Positions of the groundwater observations wells at the Krauthausen test site. The cutouts show the location of the boreholes in which ERT electrodes were installed (red circles) and transects with surface electrodes (straight red lines). The blue crosses mark the tracer injection wells. The top cutout shows the setup of the tracer experiments that are presented in this paper. The bottom cutout refers to the tracer experiment of *Kemna et al.* [2002].

in the years 2002 and 2003. During both tracer tests 140 000 l of tracer solution were injected continuously over a time period of 7 days in borehole 22 (Figure 1). The tracer solution was injected over the entire screened well section (between 3 and 11 m below the surface), which covers almost the entire saturated aquifer thickness. The injection rate was 835 l h^{-1}. In the 2002 experiment we injected a calcium chloride solution with an electrical conductivity of 6100 μS cm^{-1}, which was about a factor six more conductive than the background groundwater conductivity of 937 μS cm^{-1}. In the 2003 experiment, tracer with an electrical conductivity of 241 μS cm^{-1}, which was a factor four more resistive than the mean background groundwater conductivity of 884 μS cm^{-1} in 2003, was injected.

[11] The tracer cloud of the so-called "positive" tracer (more conductive tracer) was monitored over 78 days. The monitoring of the "negative" tracer (more resistive tracer) was completed 71 days after the beginning of injection.

[12] In both tracer experiments, we monitored the electrical conductivity of the groundwater using MLS and of the bulk sediment using ERT measurements along three transects (see Figure 1). The monitoring started with daily measurements in the first two weeks. Afterward, every 2 or 3 days was measured and at the end of the experiment, weekly measurements were done. Only 12 of 24 MLS in each observation well were sampled and the electrical conductivity at a reference temperature of 25°C of the samples was determined in the lab. To ensure that no stagnant water from inside of the tube was collected, 200 ml groundwater was purged before taking the sample. The natural background electrical conductivity of the groundwater was determined in MLS located upstream form the injection well. In order to relate the electrical conductivity of the groundwater samples at the reference temperature of 25° C with ERT derived bulk electrical conductivities, the bulk conductivities were rescaled using a temperature correction factor [*Franson*, 1985]:

$$f_T = \frac{1}{[1 + \alpha_T(T - 25)]}, \tag{1}$$

where α_T [$°C^{-1}$] is 0.0191$°C^{-1}$ for the standard 0.01 *M* KCl solution, and *T* [°C] is the temperature of the groundwater, which was 11°C during both experiments.

[13] Since the injected plumes were monitored using electrical conductivity measurements, we assumed that the transport of the electrical conductivity signal approximates the transport of an inert tracer. To test whether both the "positive" and "negative" "tracer" solutions show a similar transport behavior, lab-scale breakthrough experiments were carried out in columns packed with aquifer sediment. The sediment was taken from a drilling core between 9.5 m to 10 m below the surface. Only sediment fractions with a grain size smaller 2 mm were used. The columns were first saturated with groundwater, then charged with a 1 mol l^{-1} $CaCl_2$ pulse ("positive" tracer), and subsequently with a "negative" tracer pulse, which was a mixture of groundwater and deionized water with a ratio of 1:9. The flow rate through the columns was kept constant and amounted 0.29 ml min^{-1}. The experiments were conducted over a period of 50 h and 60 h, respectively. The electrical conductivity of the effluent was measured using a flow-through cell and corrected to a reference temperature of 25°C. In Figure 2 breakthrough curves of the positive and negative tracer pulses are shown for the column experiments. A visual inspection of the breakthrough curves confirms that the transport behavior of both tracer solutions was similar.

2.2. Electrical Resistivity Tomography

2.2.1. ERT Setup and Data Collection

[14] With ERT, an image of the spatial distribution of the bulk electrical conductivity EC_b is estimated from data sets of transfer resistance measurements. The transfer resistances, *R* (Ω) were measured using a dipole-dipole configuration in which an electrical current with strength *I* is injected using a pair of electrodes (dipole) and the electric potential difference $\Delta\Phi$, is measured between two other electrodes:

$$R = \frac{\Delta\Phi}{I}. \tag{2}$$

For the ERT measurements two transects perpendicular and one parallel to the mean flow direction were selected. In this paper we focus on the two perpendicular cross sections. The boreholes in which electrodes were installed and the ERT transects are shown in Figure 1. The first perpendicular cross section was positioned approximately 10 m downstream from the injection well and the second approximately 20 m. The image planes were spanned by four or five sampling wells equipped with electrode "strings" in the screened borehole section. Each string consisted of 16 0.5 m spaced electrodes of which 13 were situated in the saturated zone of the aquifer and used for ERT measurements. In order to increase subsurface coverage, in particular in the near surface region down to a depth of 4 m below the surface, the borehole electrodes were complemented by 32 surface electrodes with 0.75 m spacing.

[15] In this study, electrodes were paired using a combination of standard "skip-one" (surface electrodes) and "skip-two" (borehole electrodes) dipole-dipole protocols. The "skip-one" and "skip-two" configurations led to similar dipole length in both arrangements. To avoid very high potential gradients only dipoles with at least one dipole length distance to the current injection electrodes were considered for potential measurements. Only dipoles of surface electrodes or of electrodes in the same borehole were used for current injection or potential difference measurements, leading to 1770 dipole current injections per cross section. The measurements were conducted over a period of almost four months (including the measurements to determine the background bulk electrical conductivity distribution at the test site prior to the tracer experiments) using a multichannel resistivity instrument (Resecs, Geoserve GmbH Kiel, Germany).

2.2.2. Forward Modeling of ERT Data Sets

[16] In this study ERT measurements are confined to 2-D image planes. For cross-borehole electrode arrangements in a 2-D plane an ERT data set contains information predominantly about the electrical conductivity distribution in this plane, while, information content on off-plane conductivity variations is strongly limited due to the spatially biased sensitivity characteristics of individual cross-borehole ERT measurements [e.g., *Spitzer*, 1998]. Therefore, ERT data sets associated with coplanar cross-borehole electrode arrangements do not contain sufficient information

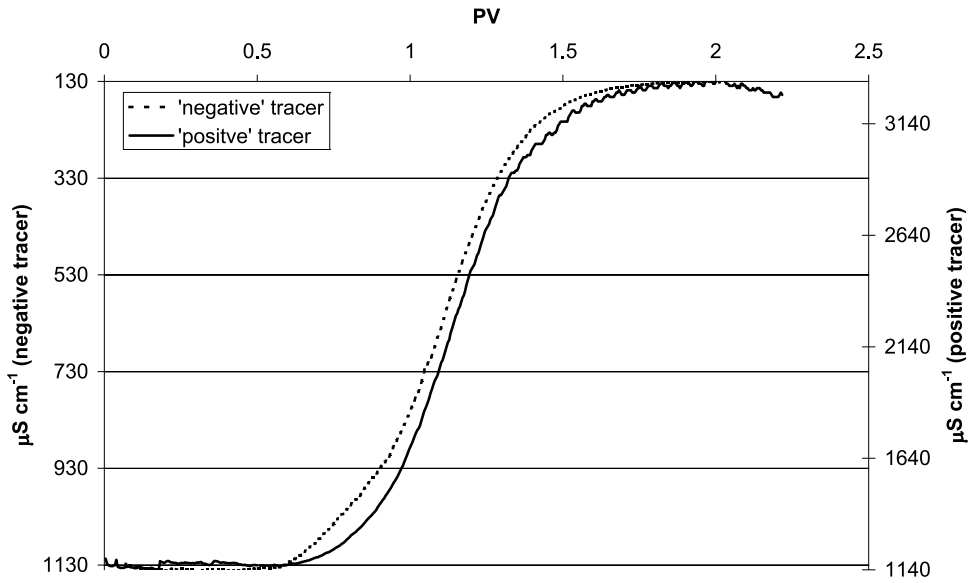

Figure 2. Breakthrough curves of the positive and negative tracers in column-scale tracer experiments plotted versus the pore volumes (PV) that leached through the columns.

that allows a 3-D inversion of the electrical conductivity distribution. For the inversion of ERT data, the electrical conductivity was assumed to be a 2-D distribution in the considered plane (image plane) that is constant in the perpendicular direction or the y direction in Figure 1. Since the forward model calculates 3-D electric potential fields in a 2-D conductivity structure, the ERT inversion is called a 2.5-D inversion. The real tracer plume has, however, a finite extension in the y direction. Because of off-plane sensitivities, the tracer plume may be detected in the resistance measurements before the tracer front actually reaches or after it passed the image plane. When the length of the tracer plume is small, resistance measurements are also influenced by off-plane regions that do not contain tracer so that the contrast or the tracer concentration in the image plane that is derived from an ERT inversion is underestimated. The impact of these artifacts on the imaging of tracer breakthrough with ERT in a reference plane was investigated indirectly in a numerical study by *Vanderborght et al.* [2005]. They simulated flow and transport and electrical resistance measurements in a 3-D heterogeneous aquifer and passed the resistance measurements to a 2.5-D ERT inversion code. Their study indicated that the assumption of a 2-D conductivity distribution did not have a large impact on the inverted tracer breakthrough. This suggests that 2.5-D inversion may be a viable approach to image transport in a heterogeneous aquifer. It must be noted that these conclusions depend on the electrode configuration, i.e., distance between electrodes and boreholes, the conductivity and the dimension of the tracer plume. The electrode configuration in the current tracer experiment was similar to that in the study by *Vanderborght et al.* [2005].

[17] Besides the assumption of constant EC_b in the y direction, it was assumed that the electrodes in the image plane are located on a perfectly planar surface that is perpendicular to the y direction. For the first cross section, the y coordinate of borehole 26 was used for the image plane and for the second cross section the y coordinate of borehole 31. The x coordinate of the ERT image plane was assumed to correspond with the distance along the lines that connect the different boreholes. Since the image planes are relatively planar and close to perpendicular to the y direction (the distances between the boreholes are close to the differences in the x coordinate), we further assumed that the ERT coordinate systems could be transformed to the Cartesian coordinate system using simple translations in the x direction.

[18] The electric potential fields and transfer resistances were calculated using the CRMOD code [*Kemna*, 2000], which uses a finite element method to solve the Poisson equation. The image plane was divided into a grid of rectangular elements (Δx = 0.375 m and Δz = 0.25 m) and the electrical conductivity within each element was assumed to be constant. The size and shape of the elements was locally adjusted so that the nodes of the elements collocate with the position of the electrodes. To improve the accuracy of the numerical solution, the rectangular elements were subdivided in four triangular elements [*Kemna*, 2000; *Kemna et al.*, 2002].

2.2.3. Inversion of ERT Data Sets

[19] Geophysical tomographic inverse problems are typically underdetermined because of the high number of model parameters. One often used precondition for finding an electrical conductivity distribution is the smoothness constraint, which requires the obtained distribution to be as smooth as possible. The inverse problem is then formulated as an optimization problem and the smoothness constraint is incorporated within an objective function.

[20] In this work, the main interest is in mapping of temporal changes in electrical conductivity and a "difference inversion" scheme [*LaBrecque and Yang*, 2001] is used that minimizes the following objective function:

$$\Psi_{diff}(\mathbf{m}) = \|\mathbf{W}[\mathbf{d} - \mathbf{d}_{in} + \mathbf{f}(\mathbf{m}_{in}) - \mathbf{f}(\mathbf{m})]\|^2 + \alpha_r \|\mathbf{R}(\mathbf{m} - \mathbf{m}_{in})\|^2, \quad (3)$$

where $\mathbf{m}$ is the parameter vector representing the log transformed electrical conductivities of the different pa-

rameter cells and $\mathbf{m}_{in}$ the reference model, $\mathbf{d}$ is the data vector of the measured and log transformed resistances and $\mathbf{d}_{in}$ is the reference data set, $\mathbf{f}$ is the operator of the forward solution, $\mathbf{W}$ is a data weighting matrix used to weight individual measurements, $\mathbf{R}$ is a matrix evaluating the roughness of $\mathbf{m} - \mathbf{m_{in}}$ in terms of its 2-D gradient, and α_r is a regularization parameter that determines the importance of the roughness of the electrical conductivity field relative to the misfit between calculated and observed resistances. The advantage of this approach is that smoothness constraint is imposed directly on the temporal model change $\mathbf{m} - \mathbf{m}_{in}$ and thus independent from time-static structures in $\mathbf{m}$ or $\mathbf{m}_{in}$. Furthermore systematic errors, which occur similarly in $\mathbf{d}$ and $\mathbf{d}_{in}$, cancel out each other. The same is true for the systematic errors in the forward models $\mathbf{f}(\mathbf{m})$ and $\mathbf{f}(\mathbf{m}_{in})$ that result for instance from small electrode misplacements, limited model discretization, and not perfectly known boundary conditions. It must be noted that only the systematic part of the model error that returns in all data sets to the same extent is canceled out in a difference inversion. Since the relation between resistance and the spatial distribution of the bulk electrical conductivity is highly nonlinear and the ERT inverse problem is strongly ill posed, systematic model and measurement errors will generally propagate differently into the inverted conductivity distribution depending on the conductivity distribution. As a consequence, the effect of the systematic errors will not be canceled out necessarily by subtracting inverted distributions. This problem is avoided in a difference inversion where systematic errors are canceled out in the measurement and model differences.

[21] Assuming uncorrelated measurement errors, the data weighting matrix is

$$\mathbf{W} = diag(1/\varepsilon_1, \ldots, 1/\varepsilon_N), \tag{4}$$

where ε_{i} is the standard deviation of the ith measurement and N is the number of measurements. ε_{i} is derived from the measured resistance R_i using the following model [*LaBrecque et al.*, 1996]:

$$\varepsilon_i = \frac{\varepsilon_{\min}}{R_i} + \varepsilon_{Ri}, \tag{5}$$

where $\varepsilon_{\min}$ (Ω) is the absolute error of the resistance measurements and $\varepsilon_{\mathrm{Ri}}$ the relative error. The reference model $\mathbf{m}_{in}$ was inverted from ERT data sets that were measured before the tracer injection using a relative error, $\varepsilon_{\mathrm{Ri}}$ of 5% and an absolute error, $\varepsilon_{\min}$, of 0.3 mΩ (equation (5)). For the difference inversion, error model parameters refer to the temporal change of the data $d_i - d_{in,i}$ and $\varepsilon_{\mathrm{Ri}}$ and $\varepsilon_{\min}$ were estimated from normal and reciprocal measurements with $\varepsilon_{\mathrm{Ri}}$ 2% and $\varepsilon_{\min}$ 0.3 mΩ. Since systematic errors cannot be derived from normal reciprocal measurements, the estimation of the error level for the absolute inversion was somehow arbitrary. It was derived from absolute inversions for a set of error levels. When the covariance between errors in two different ERT data sets, which results from systematic errors, is larger than half the random error variance, the error level is higher for the absolute than for the difference inversion. For details about the optimization algorithm that was used and the calculation of the roughness term, we refer to *Kemna et al.* [2002].

2.2.4. ERT Sensitivity

[22] The spatial resolution of ERT-derived images is a complex function of numerous factors such as the electrode layout, survey configuration, data quality, imaging algorithm, and electrical conductivity distribution. A simple and indirect approach to appraise the spatial distribution of the ERT image resolution is to map the ERT sensitivity [*Kemna et al.*, 2002]. Sensitivity describes how a local change in electrical conductivity affects a single transfer resistance measurement. The sum of all squared sensitivities with respect to a local conductivity change is an indirect measure of how well the conductivity at this location may be retrieved from the measurement data set. This squared sensitivity sum can be calculated for each parameter cell from

$$\sum_{i=1}^{N}\left[\frac{(\mathbf{A})_{ij}}{\varepsilon_i}\right]^2 = \left(\mathbf{A}^T\mathbf{W}^T\mathbf{W}\mathbf{A}\right)_{jj}, \tag{6}$$

where $\mathbf{A}$ is the Jacobi matrix with $A_{ij} = \partial d_i/\partial m_j$.

2.3. Relation Between Bulk Electrical Conductivity, EC_b, and Pore Water Electrical Conductivity, EC_w

[23] To interpret the bulk electrical conductivities of the sediment, EC_b, which are derived from ERT measurements during a tracer test, in terms of tracer concentrations, relationships between EC_b and the tracer concentration or the electrical conductivity of the pore water, EC_w need to be derived. In sedimentary rocks the conductivity of the mineral matrix is normally negligible and EC_b depends on EC_w, electrical conduction taking place at the mineral water interface (constituting a surface conductivity), and the geometry of the pore network. For sufficiently large EC_w, the surface conductivity remains constant with EC_w [e.g., *Revil and Glover*, 1998] so that the $EC_b - EC_w$ relation may be approximated fairly well by a linear calibration function [*Mallants et al.*, 1996; *Rhoades et al.*, 1989]

$$EC_b = a(\mathbf{x})EC_w + b(\mathbf{x}), \tag{7}$$

where $a(\mathbf{x})$ and $b(\mathbf{x})$ are empirical calibration parameters independent of salinity. In heterogeneous aquifers the calibration parameters depend obviously on location **x.** This was observed at the test site where the initial bulk electrical conductivity $EC_{b,in}$ varied with location despite the relatively constant background conductivity of the groundwater, $EC_{w,in}$.

[24] $EC_b, - EC_w$, calibration experiments were carried out in columns packed with aquifer sediment and charged with tracer solution of known electrical conductivity. A set of calcium chloride tracer solutions with electrical conductivities ranging from 100 μS cm^{-1} up to 5000 μS cm^{-1} was used. To investigate the spatial variability of the calibration relation, measurements were conducted with sediment from different aquifer depths, and with different fractions of gravel and sand. Samples were taken from four vertical drilling cores at intervals from 4.5 up to 9.5 m below surface for drilling cores B 63 and B 67, and from 5.5 to 6 m and 7 to 7.5 m for drilling core B 70 and from 7 to 7.5 m for drilling core B 69 (the location of the boreholes is shown in Figure 1). From the sediment that was taken in boreholes B 63 and B 67 only the sediment fractions with a grain size

smaller than 20 mm were used. The gravel and sand fractions of B 69 were first separated by sieving. Subsequently, soil columns were packed using three different gravel-sand mixtures: 70%, 50%, and 30% of sand (percentages correspond with gravimetric sand fractions). The porosity of the samples varied between 20.4% and 30.7% and the density of the packed sediment material was 2.62 g cm^{-3}. The bulk electrical conductivity EC_b was measured with TDR, and standardized to 25°C.

2.4. Stream Tube Model

[25] Similar to *Kemna et al.* [2002] and *Vanderborght et al.* [2005] we used a stream tube model to interpret the time series of the electrical conductivities that were derived from ERT and MLS. In a stream tube model, the aquifer is represented by a set of stream tubes parallel to the mean flow direction. Transport through each stream tube is described by a simple 1-D convection-dispersion process model whose parameters are constant and each tube is isolated from adjacent tubes [*Jury and Roth*, 1990]. In a stream tube model concept, locally measured tracer concentrations at a certain point $C(\mathbf{x}, t)$ are interpreted to be the result of an equivalent 1-D convection-dispersion process in a stream tube that connects the injection point with the location $\mathbf{x}$. The 1-D stream tube transport may be written as

$$\frac{\partial C(\xi,t)}{\partial t} = -v_{eq}(\mathbf{x})\frac{\partial C(\xi,t)}{\partial \xi} + v_{eq}(\mathbf{x})\lambda_{eq}(\mathbf{x})\frac{\partial^2 C(\xi,t)}{\partial \xi^2}, \qquad (8)$$

where v_{eq} and λ_{eq} are the stream tube velocity and dispersivity, respectively, and ξ is the stream tube coordinate. It must be noted that the stream tube parameters differ from the local pore water velocity and dispersivity at the location where the breakthrough is measured. The stream tube parameters synthesize the time series of concentrations and must be viewed as normalized temporal moments of the breakthrough curves or as parameters of an equivalent convection-dispersion process that leads to the same temporal moments as the observed breakthrough curve. The advantage of using stream tube parameters instead of temporal moments is that the spatial variability of the parameters within an image plane and between different image planes is easier to interpret and compare. The variability of v_{eq} across a reference plane is a measure of plume distortion as a result of spatial variations of water flow. The averaged value of λ_{eq} represents the dilution of the locally observed concentrations due to mixing along the stream tube trajectory. Direct relations between the spatial variability of v_{eq} and the hydraulic conductivity can be derived and the average λ_{eq} can be related to the local-scale dispersion constant and the spatial variability of the hydraulic conductivity [*Bellin and Rubin*, 2004; *Vanderborght et al.*, 2005; *Vanderborght et al.*, 2006].

[26] Since the stream tube model interprets locally measured breakthrough curves and quantifies their spatial variability, it is more powerful to quantify transport heterogeneity than an effective macroscale dispersion model, which could be parameterized from spatially averaged breakthrough curves. A macroscale dispersion model assumes a uniform aquifer and the impact of aquifer heterogeneity on transport is lumped into the macroscale dispersion tensor. Because of this averaging and lumping, the mixing and the spatial variability of the transport process cannot be derived from the macroscale dispersion coefficients.

[27] The parameters v_{eq} and λ_{eq} are obtained by fitting the solution of the 1-D convection-dispersion equation to the locally measured, i.e., by a MLS or within a pixel of the ERT image plane, breakthrough curve. We assumed that the transport distance in each stream tube is the same and corresponds with the distance from the injection well to the image plane. As a consequence, we assumed a mean uniform flow in the y direction and we neglected the effect of lateral and upstream tracer movement during the tracer injection and the vertical displacement resulting from density driven flow. In other words, we assume that the transfer time or v_{eq} and the mixing or λ_{eq} from the injection well to an observation point in an image plane are hardly affected by lateral and downward displacement. The impact of this assumption on the derived stream tube parameters was assessed using 3-D flow and transport simulations in a homogeneous aquifer. Since the lateral and backward displacement during the tracer injection were considerably larger than the vertical displacement due to density driven flow, density driven flow was not considered in the 3-D simulations.

[28] For a step input at the inlet of the stream tube with an initial concentration C_{in}, and assuming that the ξ coordinate aligns with the y coordinate, the solution of the 1-D transport equation, equation (8), is [*Toride et al.*, 1999]

$$\begin{aligned} C(y,t) - C_{in} = {} & \\ & \frac{(C_0 - C_{in})}{2}\left[erfc\left(\frac{y - v_{eq}t}{\sqrt{4v\lambda_{eq}t}}\right) + \exp\left(\frac{y}{\lambda_{eq}}\right)erfc\left(\frac{y + v_{eq}t}{\sqrt{4v_{eq}\lambda_{eq}t}}\right)\right] \\ & - w\frac{(C_0 - C_{in})}{2}\left[erfc\left(\frac{y - v_{eq}(t - t_0)}{\sqrt{4v_{eq}\lambda_{eq}(t - t_0)}}\right)\right. \\ & \left. + \exp\left(\frac{y}{\lambda_{eq}}\right)erfc\left(\frac{y + v_{eq}(t - t_0)}{\sqrt{4v_{eq}\lambda_{eq}(t - t_0)}}\right)\right], \end{aligned} \qquad (9)$$

where t_0 is the duration of the solute input, i.e., 7 days, C_0 the input concentration at the stream tube inlet and w a weighting factor, which is 0 for $t < t_0$ and 1 for $t \geq t_0$, and y is the direction of the mean flow. Because of lateral mixing of the tracer solution with the groundwater and the small lateral extent of the borehole in which the tracer solution was injected, the tracer solution is more diluted than in the case of purely one-dimensional transport. This leads to a smaller observed C_0 in a stream tube than the injected C_0. In our experiments, we stopped the water and solute injection simultaneously. After the injection, the flow field returned to the ambient groundwater flow and pushed back the tracer that was injected upstream of the injection well. As a consequence, the injection time in a stream tube appears to be longer than the duration of the solute injection. We kept, however, the injection time constant, which is reasonable when the increase in injection time is small compared with the travel time to the image plane. The additional tracer mass that entered the stream tube after the injection stopped was accounted for using a larger apparent C_0 than the real C_0. Therefore, also C_0 was fitted to account for additional

dilution due to lateral mixing with groundwater and the upstream tracer that entered the stream tube after the tracer injection stopped.

[29] Stream tube parameters were derived from pixel-scale breakthrough curves in the ERT image planes and compared with stream tube parameters derived from MLS data from the boreholes situated at the ERT image planes. Since we measured electrical conductivity, the tracer "concentration" C that we measured represents an amount of electrical charge carried by ions per volume of water. Instead of fitting equation (9) to solute concentrations, equation (9) was fitted to relative changes in bulk electrical conductivity (ERT data), relative to the initial bulk conductivity, or to relative changes in electrical conductivity of the pore water (MLS data). If the electrical conductivity is related linearly to the electrical charge concentration, it is trivial that equation (9) with the same parameters v_{eq} and λ_{eq} also describes the breakthrough curve of relative changes in electrical conductivity. Then, $C_0 - C_{in}$ represents the relative change in electrical conductivity when the initial groundwater solution is replaced by the injected tracer solution. For the ERT data, $C_{0,ERT} - C_{in,ERT}$ is

$$C_{0,ERT}(\mathbf{x}) - C_{in,ERT}(\mathbf{x}) = \frac{EC_{b,0}(\mathbf{x}) - EC_{b,in}(\mathbf{x})}{EC_{b,in}(\mathbf{x})} = \frac{EC_{w,0} - EC_{w,in}}{EC_{w,in} + b(\mathbf{x})/a(\mathbf{x})}, \quad (10)$$

where $EC_{b,0}(\mathbf{x})$ is the bulk electrical conductivity when the pore space at location $\mathbf{x}$ is filled with the injected tracer solution in the stream tube, C_0, with an electrical conductivity $EC_{w,0}$, and $EC_{b,in}(\mathbf{x})$ is the initial bulk electrical conductivity at $\mathbf{x}$, and $b(\mathbf{x})$ and $a(\mathbf{x})$ are the parameters at location $\mathbf{x}$ of the petrophysical relation (equation (7)) that relates EC_b and EC_w. Since $C_{0,ERT} - C_{in,ERT}$ is derived from fitting equation (9) to relative changes in EC_b, the parameters $a(\mathbf{x})$ and $b(\mathbf{x})$ do not need to be known to derive the stream tube parameters v_{eq} and λequation The PROC NLIN procedure of the SAS/STAT® statistical software package was used to fit equation (9) to the ERT and MLS data. Since stream tube model parameters can only be determined at locations where tracer breakthrough takes place, only parameters at locations where the fitted $C_{0,ERT} - C_{in,ERT}$ was above a threshold value were retained.

2.5. Tracer Balance Calculations

[30] The amount of tracer that crosses a reference plane which is perpendicular to the mean flow direction can be calculated as

$$M = \int q_y(\mathbf{x})(C(\mathbf{x},t) - C_{in})dtdxdz, \quad (11)$$

where $q_y(\mathbf{x})$ is the water flux at location $\mathbf{x}$ in the reference plane. A problem with the application of equation (11) is that $q_y(\mathbf{x})$ is generally not known. However, numerical simulations in heterogeneous aquifers [e.g., *Vanderborght et al.*, 2005, Figure 8] indicated that the time integral of flux-weighted and nonweighted concentrations are similar. This implies that the time integral of local concentrations is not correlated with the local water flux. As a consequence, $q_y(\mathbf{x})$ was here approximated by the mean flux, $\langle q_y \rangle$, through the reference plane:

$$M = \langle q_y \rangle \int (C(\mathbf{x},t) - C_{in})dtdxdz. \quad (12)$$

Assuming that electrical conductivity of the tracer solution is linearly related to the tracer concentration, the tracer recovery, M/M_0 can be expressed in terms of electrical conductivities of the groundwater as

$$\frac{M}{M_0} = \frac{\langle q_y \rangle \int (EC_w(\mathbf{x},t) - EC_{w,in})dtdxdz}{V_0(EC_{w,0} - EC_{w,in})}, \quad (13)$$

where M_0 is the injected tracer amount and V_0 is the injected tracer volume. Using equation (7) in equation (13), the tracer recovery can be expressed in terms of the bulk electrical conductivity as

$$\frac{M}{M_0} = \frac{\langle q_y \rangle \left[EC_{w,in} + \frac{b}{a}\right]}{V_0(EC_{w,0} - EC_{w,in})} \int \frac{EC_b(\mathbf{x},t) - EC_{b,in}(\mathbf{x})}{EC_{b,in}(\mathbf{x})} dtdxdz. \quad (14)$$

In the derivation of equation (14), it was assumed that the parameter b/a does not change with location. However, if $b(\boldsymbol{x})/a(\boldsymbol{x})$ is small compared with $EC_{w,in}$, i.e., when the initial bulk EC is determined mainly by the electrical conductivity of the pore water, a violation of this assumption does not have a large impact on the calculated tracer recovery. This implies that for the calculation of the tracer recovery using equation (14), detailed and accurate information about the petrophysical relation $EC_b - EC_w$ and its spatial variability is not required. If the times series of relative changes in EC_b can be described using equation (9), then the time integral corresponds with $[C_{0,ERT}(\mathbf{x}) - C_{in,ERT}(\mathbf{x})]t_0$ and equation (14) can be written as

$$\frac{M}{M_0} = \frac{\langle q_y \rangle \left[EC_{w,in} + \frac{b}{a}\right] t_0}{V_0(EC_{w,0} - EC_{w,in})} \int (C_{0,ERT}(\mathbf{x}) - C_{in,ERT}(\mathbf{x}))dxdz. \quad (15)$$

2.6. Transport Simulations in a Homogeneous Aquifer

[31] Three-dimensional flow and transport were simulated during a tracer test in a homogeneous aquifer in order to evaluate the effect of nonuniform flow conditions that are induced by the tracer injection on the stream tube transport parameters and the relative change in electrical conductivity, $C_{0,ERT} - C_{in,ERT}$, which is derived from fitting equation (9) to time series of ERT derived EC_b. The simulation domain was 40 m long, 24 m wide, and 12 m deep. No-flow boundary conditions were defined at the bottom, top and the lateral surfaces of the simulation domain and constant heads were defined at the front and back surface resulting in a hydraulic gradient of 0.002. The hydraulic conductivity was 0.0015 m s^{-1}, the porosity 0.27, and the longitudinal and transverse dispersivity 0.9 m and 0.09 m, respectively. As in the tracer experiment, 140 m^3 of tracer solution was injection over a period of 7 days in an injection well between 2.75 and 10.5 m depth. Simulated local breakthrough curves

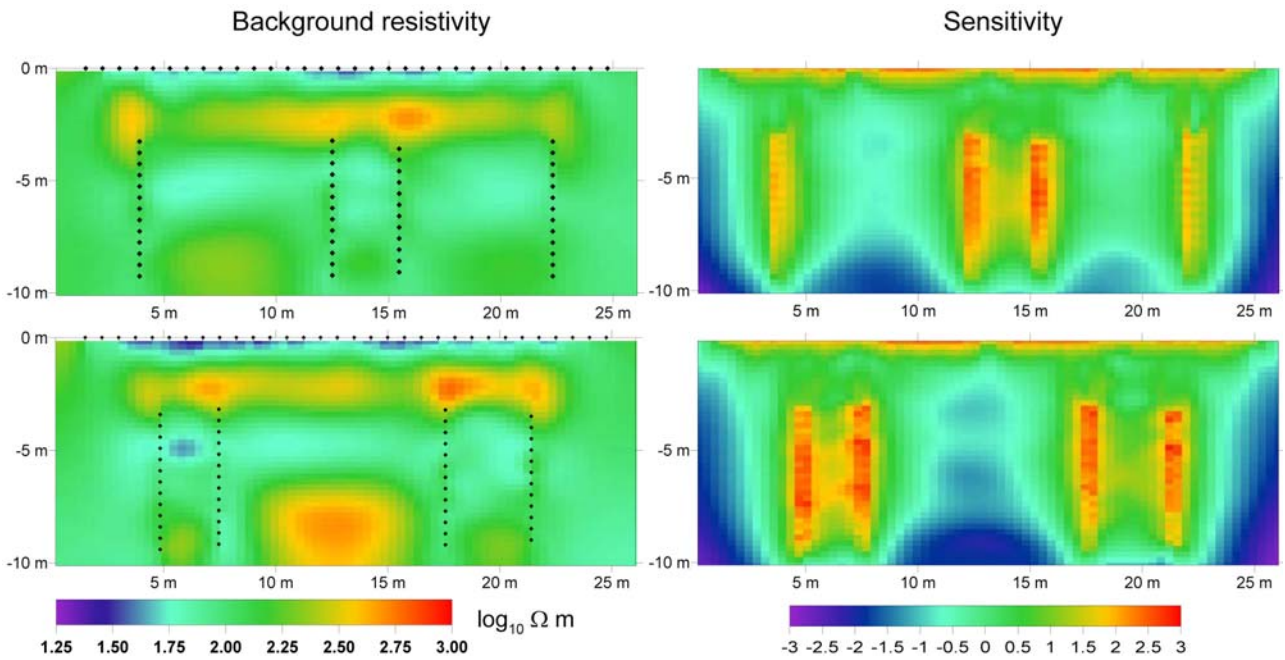

Figure 3. (left) ERT background images of the bulk electrical resistivity distribution and (right) the corresponding sensitivity distributions in the (top) first and (bottom) second cross sections. Resistivities are given in $\log_{10}$ Ω m. The locations of the electrodes are marked by the black dots.

at two reference surfaces at 11 m and 21 m downstream of the injection well were fitted by the stream tube model, similar to the breakthrough curves that were observed during the real tracer test.

3. Results

[32] This section is organized as follows. First the ERT sensitivity for the employed electrode arrangement and measurement as well as the distribution of the background EC_b are presented. Then the results of the lab-scale calibration experiments to determine the $EC_b - EC_w$ relation are given. In a next part, the tracer breakthroughs in the ERT cross sections and in the MLS are compared for both the positive and negative tracer tests. In the last two parts, fitted transport model parameters and calculated tracer recoveries are presented.

3.1. ERT Background Images and Sensitivity

[33] The ERT background images, $\mathbf{m}_{in}$, which are used in the difference inversion equation (3), and the corresponding sensitivity distributions, equation (6), are shown in Figure 3. Basically, the background distribution reflects the lithological situation at the test site with a relatively resistive layer at a depth about −2 m depth corresponding with the unsaturated gravel sediment below the top loess soil layer. Below −2 m, the saturated zone of the aquifer is marked by a decrease in resistivity. Between −4 and −5 m depth appears a layer with slightly lower resistivities, which corresponds with a layer with a higher sand fraction. The ERT-derived vertical resistivity or conductivity profile corresponds with profiles that were derived from cone penetration tests [*Tillmann et al.*, 2008]. As to be expected, overall sensitivity and resolution decrease dramatically toward the bottom of a cross-borehole ERT plane and toward the middle between the boreholes [*Ramirez et al.*, 1993].

3.2. $EC_b - EC_w$ Relation

[34] Figure 4 shows the relation between EC_w and EC_b for three columns that were packed with aquifer material from the drilling core 70. These plots demonstrate that a linear relation between EC_w and EC_b may be assumed for the range of pore water conductivities in this study (EC_w ranges from 241 to 6100 μS cm^{-1}). Figure 4 also indicates that the intercept of the $EC_b - EC_w$ relation is small compared with $EC_{b,in}$, i.e., the bulk EC for the background $EC_{w,in}$ (≈900 μS cm^{-1}).

[35] In Table 1, the parameters of the linear $EC_b - EC_w$ relation that were derived in columns packed with aquifer sediment are listed. The parameter $a(\mathbf{x})$ varied between 0.15 and 0.21 and increased with decreasing gravel and increasing sand content. The intercept $b(\mathbf{x})$ varied between 12 and 36 μS cm^{-1} but did not show a clear relation with sand or gravel contents. Based on these calibration experiments, $EC_{b,in}$ at a reference temperature of 25°C ranges from 150 to 210 μS cm^{-1}. This corresponds with a range of bulk resistivities, ρ, at 11°C from 65 to 90 Ωm or of log10ρ from 1.8 to 1.95, which is considerably smaller than the range of log10ρ in Figure 3. For the layers between approximately −4 and −11 m depth (layers D and E in the work by *Tillmann et al.* [2008]) the range of resistivities derived from cone penetration tests was between 65 and 140 Ωm (log10ρ ranges from 1.8 to 2.15).

3.3. Patterns of Tracer Breakthrough at the Two ERT Image Planes

[36] In Figures 5 and 6, the spatiotemporal patterns of changes in relative bulk electrical resistivity ("negative"

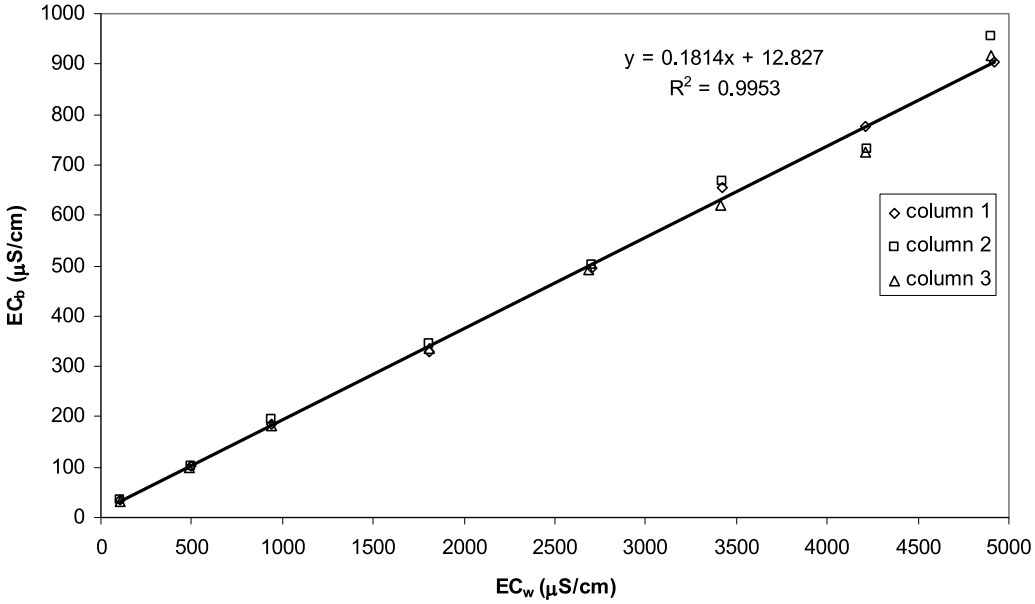

Figure 4. Relation between electrical conductivity of the pore fluid, EC_w, and the bulk electrical conductivity, EC_b, in three replicate columns that were packed with aquifer sediment (drilling well 70, 5.5–6 m depth).

tracer 2003) and bulk electrical conductivity ("positive" tracer 2002) in the two image planes are shown for several time steps after the start of injection. The relative changes in bulk resistivity are defined as

$$\Delta_r \rho = \left[\frac{1/EC_b - 1/EC_{b,in}}{1/EC_{b,in}} \right], \tag{16}$$

and the relative changes in bulk conductivity as

$$\Delta_r EC_b = \left[\frac{EC_b - EC_{b,in}}{EC_{b,in}} \right]. \tag{17}$$

The relative changes in bulk resistivity and conductivity obtained with ERT were compared with relative changes in water resistivity and conductivity obtained from the MLS, which are represented by vertical bars in Figures 4 and 5. With respect to the arrival times of the tracer plumes at the image planes and the magnitude of the maximum relative changes in resistivity and conductivity, the MLS data show some agreement with the ERT data. However, differences obviously exist. In the first image plane at 10 m downstream from the injection well, the ERT images show a lateral spreading of the plume already at 7 days after the beginning of the injection whereas the tracer was only detected in the multilevel samplers straight downstream from the injection well but not in the adjacent boreholes. During the positive tracer test, a tail of high conductivities was observed in MLS in the lower part of the aquifer near to the aquifer base in both image planes, e.g., from day 24 until day 44 in the first cross section (Figure 5, right) and from day 36 until day 65 in the second cross section (Figure 6, right). However, this tailing was not detected in the ERT images. Although the ERT sensitivity decreased toward the bottom of the aquifer (Figure 3), it was still relatively high at the bottom part of the boreholes which makes it unlikely that high electrical conductivities in a sufficiently large volume around the borehole would remain undetected by ERT. The tailing observed in the MLS could also suggest that the salt tracer sank within the borehole and that MLS in the bottom part of the aquifer were not well connected to the groundwater flow.

[37] In the second cross section (Figure 6), the ERT images appear to be more diffuse than in the first cross section (Figure 5). The conductivity and resistivity contrasts were smaller as a result of successive dilution with increasing distance from the injection source. For the negative tracer experiment, the peak of the tracer breakthrough in the ERT images at the second cross section was observed after 21 days and corresponded with a relative change in ρ of about 100%. This was about twice the change in the MLS

Table 1. Parameters of the Linear $EC_w - EC_b$ Calibration Relation, Equation (7), for Different Sand-Gravel Mixtures Taken From the Krauthausen Aquifer Sediment

Drilling Well and Depth	Sand (%)	Gravel (%)	a	b (S m^{-1})	Porosity
B63/67, 4.5–9.5 m	100	0	0.2070	0.0018	28.80
B63/67, 4.5–9.5 m	100	0	0.1916	0.0018	27.13
B63/67, 4.5–9.5 m	100	0	0.2072	0.0021	27.14
B69, 7–7.5 m	100	0	0.2098	0.0017	30.06
B69, 7–7.5 m	100	0	0.2191	0.0012	29.82
B69, 7–7.5 m	100	0	0.2048	0.0020	30.34
B69, 7–7.5 m	70	30	0.1798	0.0017	26.51
B69, 7–7.5 m	70	30	0.1703	0.0012	25.49
B69, 7–7.5 m	50	50	0.1648	0.0015	25.17
B69, 7–7.5 m	50	50	0.1534	0.0023	25.63
B69, 7–7.5 m	30	70	0.1509	0.0016	25.42
B69, 7–7.5 m	30	70	0.1541	0.0015	24.75
B70, 5.5–6 m	66.3	33.7	0.1782	0.0012	25.19
B70, 5.5–6 m	62.0	38.0	0.1840	0.0014	24.52
B70, 5.5–6 m	65.9	34.1	0.1821	0.0012	24.44
B70, 9–9.5 m	61.6	38.4	0.1551	0.0022	25.24
B70, 9–9.5 m	62.9	37.1	0.1563	0.0033	22.89
B70, 9–9.5 m	61.1	38.9	0.1550	0.0036	20.40

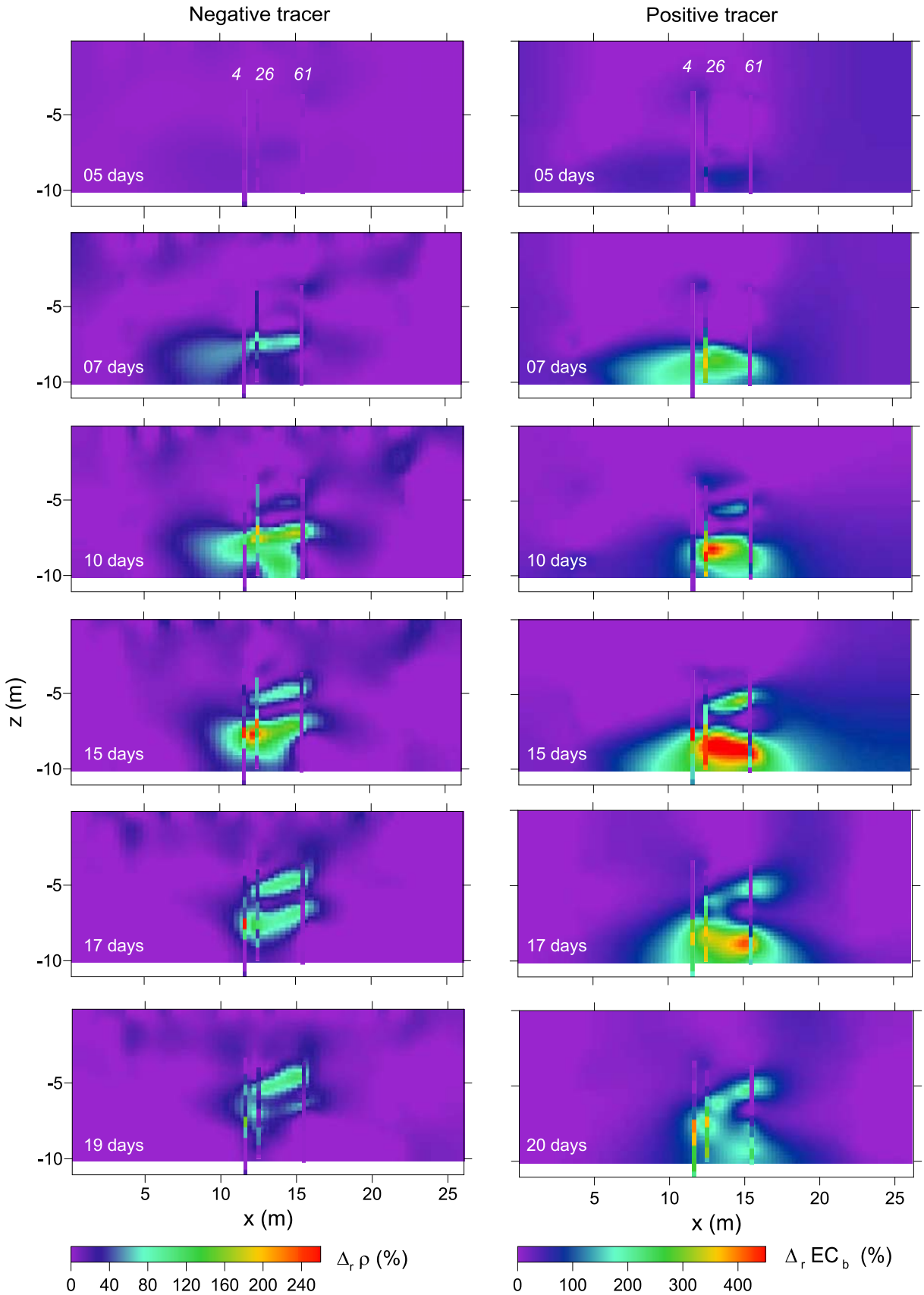

Figure 5. Relative changes in (left) bulk resistivity ρ (in %) for the "negative" tracer and (right) bulk conductivity EC_b (in %) for the "positive" tracer test in the first cross section for different days after the beginning of the tracer injection. Vertical bars represent changes measured by multilevel samplers, and italic numbers are the borehole numbers.

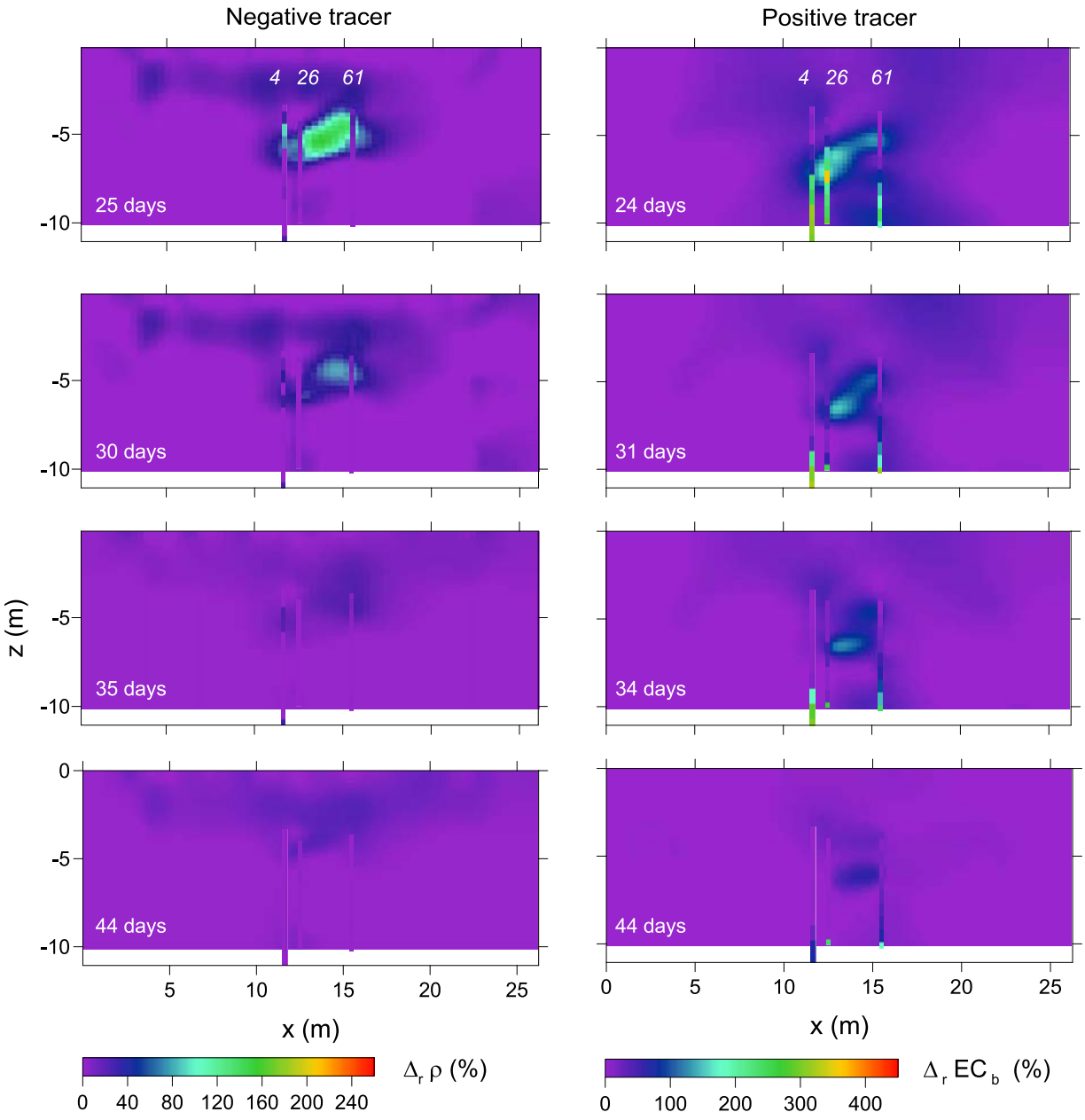

Figure 5. (continued)

and about half the change that was observed in the first cross section. For the positive tracer experiment, the peak of the relative changes in EC_b of 220% in the ERT images of the second cross section is also about half of that in the first cross section but smaller than the change observed in the MLS, which is larger than 300%. For the negative tracer experiment, higher and temporally varying resistivities were observed in the upper zone of the ERT image plane which represents the unsaturated zone. These observations might be due to temporal moisture content changes associated with rainfall events and dry periods during the monitoring period.

[38] The tracer cloud that was monitored with ERT at the second cross section spread out to a lesser horizontal extent as would be expected based on the MLS. For the positive tracer experiment, the MLS indicate that the tracer plume extended laterally from boreholes 38 to 62 (see Figure 1 for the location of the boreholes). From day 15 until day 36 during the positive tracer experiment, a considerable breakthrough was observed in the MLS at borehole 38. This borehole was not equipped with ERT electrodes since it was not fully screened. The ERT images also suggest that the tracer plume extended laterally from borehole 38 to 62 but the ERT-derived changes in electrical conductivity were much smaller than the ones observed in the MLS in borehole 38. This may be explained by the low ERT sensitivity at the location of borehole 38 (see Figure 3). The lateral

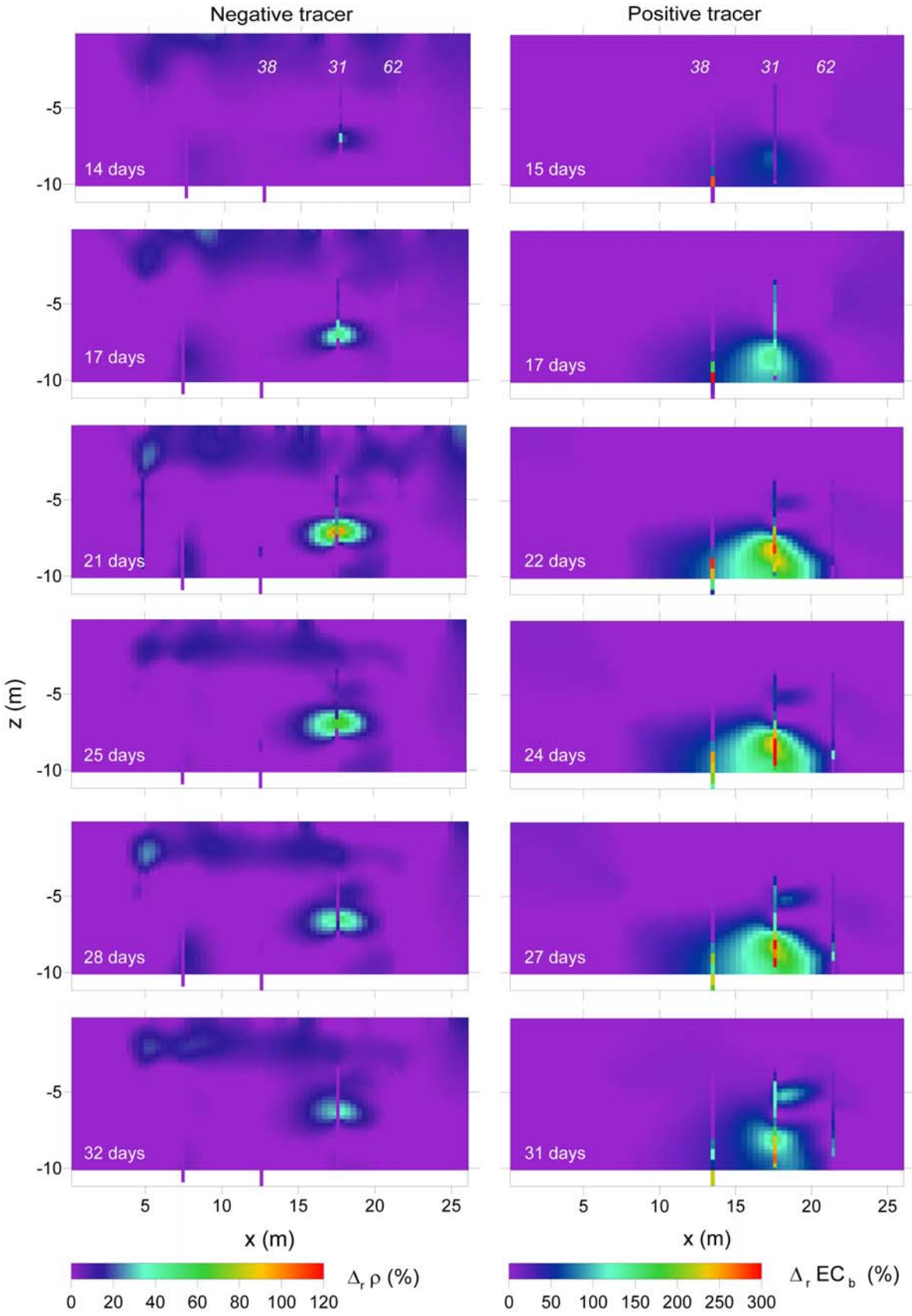

Figure 6. Relative changes in (left) bulk resistivity ρ (in %) for the "negative" tracer and (right) bulk conductivity EC_b (in %) for the "positive" tracer test in the second cross section for different days after the beginning of the tracer injection. Vertical bars represent changes measured by multilevel samplers, and italic numbers are the borehole numbers.

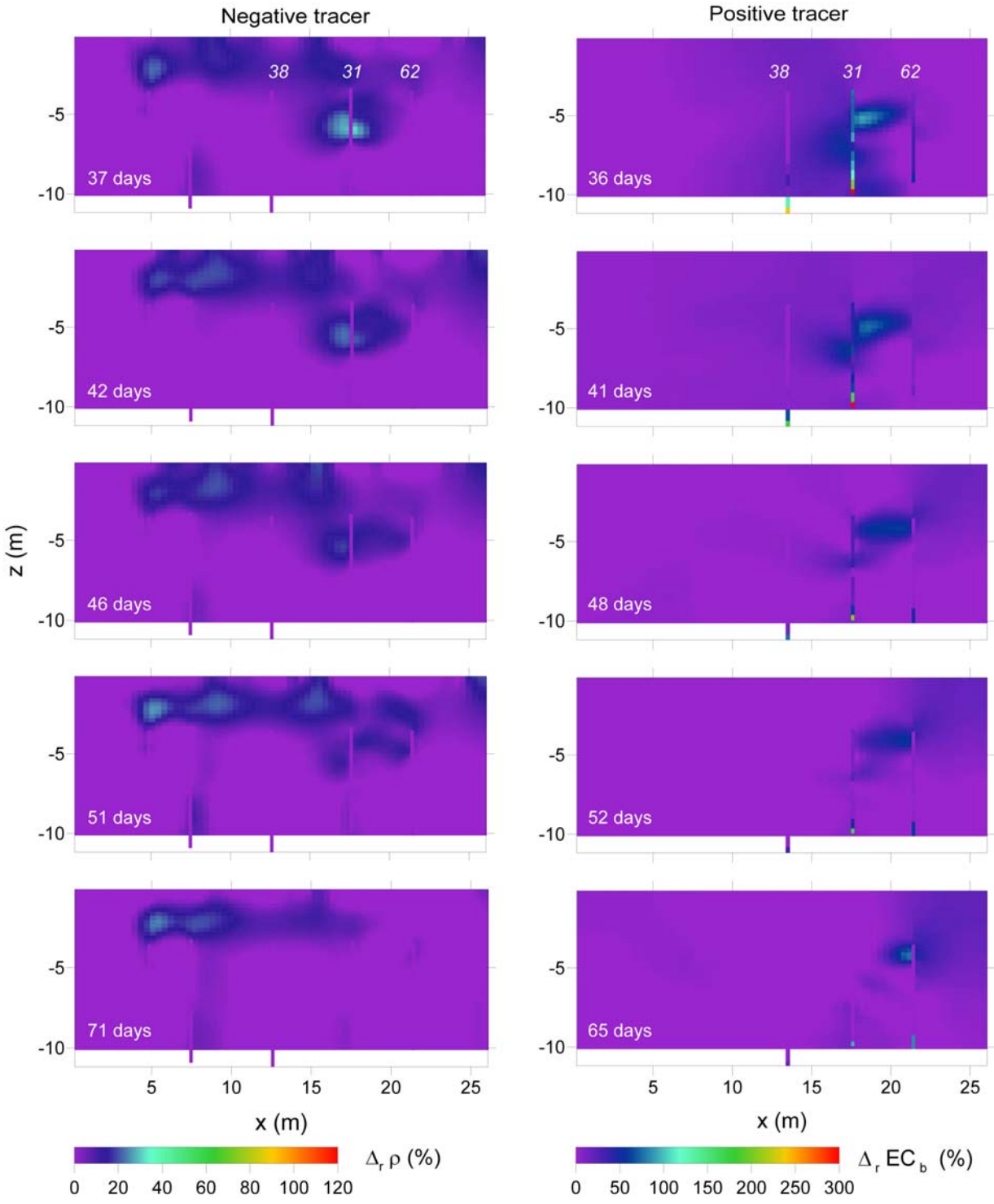

Figure 6. (continued)

extent of the negative tracer plume was considerably smaller than that of the positive plume; however, a small breakthrough of tracer observed at borehole 38 from day 21 until day 25 also suggests that the ERT images underestimated the lateral extent of the tracer plume.

[39] Comparing the negative and positive tracer experiments shows that the negative tracer moved primarily through the middle central part in the ERT image plane whereas the positive tracer sank down to the lower central part of the ERT image plane. Generally, the downward sinking of the positive tracer was accompanied by a larger

lateral extent of the estimated tracer plume, while the lower part of the negative tracer cloud showed an upward trend. For the positive tracer a pronounced tailing was observed. The patterns of the breakthrough in both ERT image sequences and for both tracer experiments also show some interesting similarities that point at signatures of aquifer heterogeneity on tracer transport. In both experiments, a plume splitting was observed in the first ERT cross section. The breakthrough in the upper and middle part of the first cross section was delayed in comparison with the breakthrough in the lower part of the aquifer. This splitting was also observed in the second cross section but not so clearly for the negative tracer experiment. The small signal-to-noise ratio in the negative tracer experiment possibly inhibited seeing the relatively small and more diluted breakthrough in the middle and upper part of the second cross section. The plume splitting could, however, not be observed in the MLS data.

3.4. Comparison Between Local Breakthrough Curves

[40] In Figure 7, changes in bulk electrical conductivity, ΔEC_b, which were derived from ERT images and calculated from the electrical conductivities measured in the MLS are shown for wells 26 and 31. These wells are located in the center of the tracer plume trajectories. Based on the calibration experiments, (Table 1) $a = 0.18$ was chosen to calculate ΔEC_b from MLS measurement of EC_w.

[41] During the positive tracer test, the main tracer breakthrough in well 26 was detected by both the MLS and ERT in the middle and lower parts of the aquifer. In this well and during the positive tracer test, the mean arrival of the breakthrough occurred earlier in the deeper part of the aquifer (MLS from −7.58 to −9.38 m) than in the upper part of aquifer. However, an earlier breakthrough and higher peak concentrations were observed in the MLS at −6.38 m compared with the ERT derived breakthrough curve. The breakthrough curves (BTCs) derived from the lowest parts in the aquifer show a good agreement between MLS and ERT concerning to peak magnitude and shape of the BTCs. During the negative tracer test, the main tracer mass in well 26 was detected in the middle aquifer zone. Consistent with the positive tracer test, the ERT derived BTCs showed an earlier arrival in the deeper part of the aquifer and a later arrival in upper part of the aquifer. This is in contrast with the MLS that do not show this consistency in arrival times between the two experiments. The MLS showed similar peak arrival times at different depths in the negative tracer test but a delay in arrival times or peak concentrations in the upper part of the aquifer for the positive tracer test. A similar difference between the MLS and ERT derived BTCs was observed during the negative tracer test in well 31, which is located further downstream. For the positive tracer test, the MLS at well 31 showed double peak BTCs in the upper part of the aquifer (−6.35 m and above). Also in the deeper part of the aquifer (at −9.35 and −8.75 m) a small double peak was observed. The first peak in the upper part of the aquifer corresponds with the raise of concentrations in the deeper part of the aquifer. The second peak in the upper part of the aquifer arrived later than the peak in the deeper part and its arrival is more consistent with the peak arrival in the ERT images, which show an earlier arrival in the deeper than in the upper part of the aquifer. The consistency between the ERT-derived BTCs for the positive and negative tracer experiments is less given for well 31 than for well 26. At −8.75 and −9.35 m depth no breakthrough was observed using ERT during the negative tracer test whereas the highest peak concentrations were observed at these depths during the positive tracer test. On the other hand at −6.35 m depth no significant breakthrough occurred during the positive tracer test whereas considerable breakthrough was observed during the negative tracer test. These differences are on one hand due to the different tracers with the positive tracer sinking downward toward the aquifer base. On the other hand, the smaller tracer contrast in the negative tracer experiment may have resulted in a lower resolution of the ERT images so that the narrow region (at −6.35 m) with lower tracer concentrations was smoothed out in the inversion. It should also be noted that resistive anomalies are generally less resolved because current tends to channel around them. This leads to different sensitivities, sampling volumes, and spatial resolutions in the ERT data sets for the positive and negative tracer tests.

3.5. Stream Tube Parameters

[42] The stream tube velocity v_{eq} and dispersivity λ_{eq} for the positive and negative tracer tests and for the transport simulations in the homogeneous aquifer are shown in Figures 8 and 9 for the first and second image planes, respectively. The vertical bars in Figures 8 and 9 represent v_{eq} and λ_{eq} that were derived from the MLS data. The mean and coefficient of variation CV of v_{eq} and λ_{eq} are given in Table 2.

[43] Simulations in the homogenous aquifer demonstrated that lateral and backward movement of the tracer during the injection lead to smaller stream tube velocities v_{eq} (0.82 m d^{-1} for reference plane 1 and 0.88 m d^{-1} for reference plane 2) than in the case of uniform flow (0.96 m d^{-1}). The spatial variation of the stream tube velocities in the reference planes was, however, small. Nonuniform flow conditions also had some impact on the derived stream tube dispersivities, which were on average somewhat larger than the longitudinal dispersivity that was used in the transport simulations (0.9 m). When compared with the variability of the stream tube parameters that were derived from MLS and ERT, the effect of nonuniform flow on these parameters is, however, small.

[44] For both the positive and negative tracer tests, v_{eq} derived from the ERT data sets were higher in the lower part of the aquifer. However, v_{eq} was somewhat higher for the "negative" than for the "positive" tracer test. The v_{eq} derived from the MLS were only in rough accordance with those derived from ERT. The average v_{eq} derived from MLS at the first image plane were considerably smaller than those derived at the second image plane and the ERT derived ones, which were on average similar for the two reference planes and the two tracer experiments. The relatively large deviation in average v_{eq} derived from MLS at the different image planes indicates that MLS did not sample a sufficiently large cross section of the aquifer to obtain a representative image of the average breakthrough. Since with ERT, the entire cross section between the boreholes was imaged, albeit with a varying spatial resolution, a more representative observation of the tracer breakthrough was obtained with this method. The MLS-derived v_{eq} neither showed a clear sep-

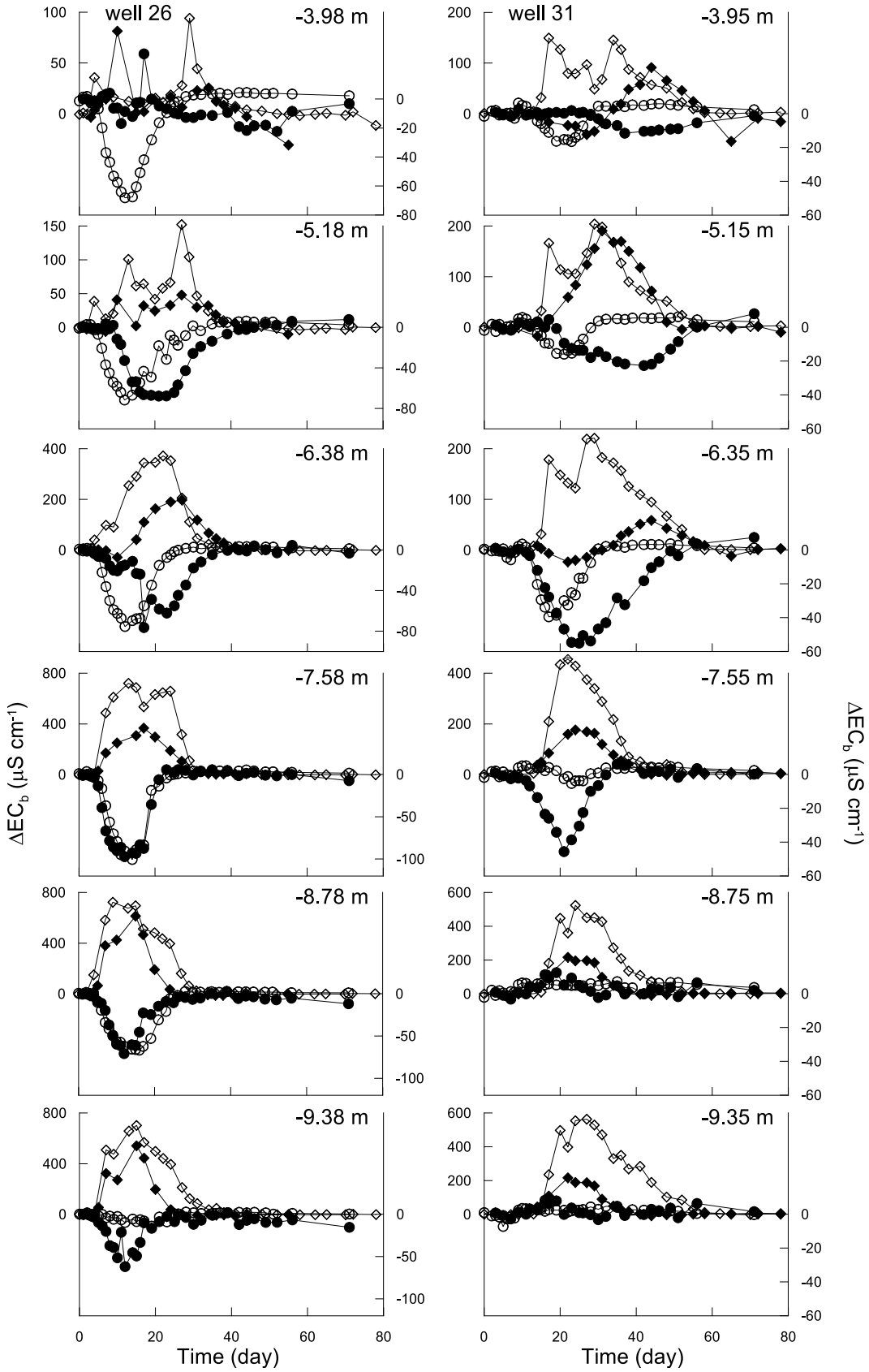

Figure 7. Absolute change in bulk electrical conductivity during the positive (positive changes) and negative (negative changes) tracer experiment measured with MLS (open symbols) and ERT (solid symbols) at (left) well 26 (first ERT image plane) and (right) well 31 (second image plane).

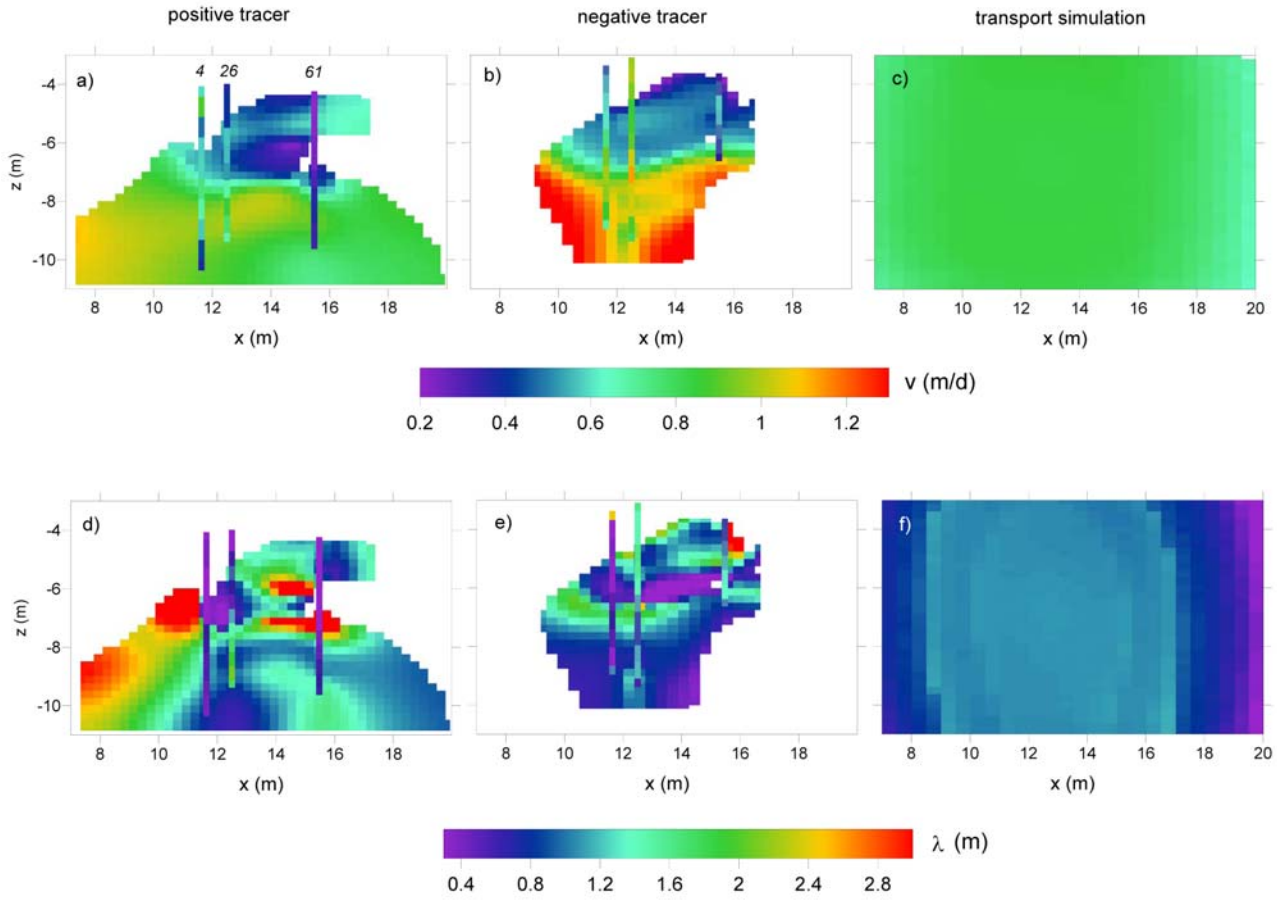

Figure 8. Stream tube (a–c) velocities, v_{eq}, and (d–f) dispersivities, λ_{eq}, in the first ERT image plane for the positive (Figures 8a and 8d) and negative (Figures 8b and 8e) tracer tests and for the transport simulation in a homogeneous aquifer (Figures 8c and 8f). Vertical bars represent stream tube parameters that were derived from breakthrough curves measured with MLS (italic numbers are the well numbers).

aration between the lower and upper part of the aquifer nor a common pattern in the two tracer experiments. For example, in well 4, there was a rapid breakthrough during the "positive" tracer test between −4 and −5 m depth. This was neither observed in the "negative" test nor in the ERT data. In well 26, there was a slower breakthrough during the "positive" experiment between −4 and −7 m depth than in well 4, whereas the opposite is true for the "negative" tracer test. These inconsistencies in the MLS data point at some fundamental problems with using such local sampling methods to monitor tracer tests and characterize transport in heterogeneous aquifers.

[45] The patterns of the ERT-derived stream tube dispersivities, λ_{eq}, do not show such a clear zonation as the patterns of v_{eq} do. However, regions with large λ_{eq} were found in regions where the gradient in v_{eq} was large. This is in accordance with numerical experiments in synthetically generated heterogeneous aquifers [*Vanderborght et al.*, 2005] and is explained by the spatial averaging in the ERT inversion which results in a numerical or artificial mixing and consequently an overestimation of λ_{eq} in regions with large gradients in *v*equation The numerical mixing led to an overestimation of the average λ_{eq} by ERT in the synthetic experiment. Except for the first image plane and the positive tracer experiment, the MLS-derived λ_{eq} do not indicate a strong overestimation of λ_{eq} by ERT in the field experiments. However, the slight decrease of the average λ_{eq} with increasing travel distance, might be explained by a an increased dilution of the tracer plume with travel distance which decreases local concentration and bulk electrical conductivity gradients and therefore leads to a smaller numerical mixing [e.g., *Singha and Gorelick*, 2005]. The numerical mixing, which leads to an overestimation of λ_{eq}, may be counteracted by the ERT inversion that does not pick up small concentrations. This could be an additional explanation for the relatively small overestimation of λ_{eq} by ERT and the decrease of λ_{eq} with travel distance.

3.6. Recovered Tracer

[46] The tracer balances M/M_0 calculated using equation (15) are given for the two tracer experiments and the two image planes in Table 3. To calculate M/M_0, the mean flow rate across the image plane $\langle q_y \rangle$, was estimated from the mean stream tube velocity, $\langle v_{eq} \rangle$ (see Table 2) and multiplied with the mean aquifer porosity, $\varphi = 0.27$. The petrophysical parameters a and b (equation (7)) were set to 0.18 and 17.5 μS cm^{-1}, respectively (Table 1). The parameter $C_{0,ERT} - C_{in,ERT}$ (equation (10)) was derived for each pixel

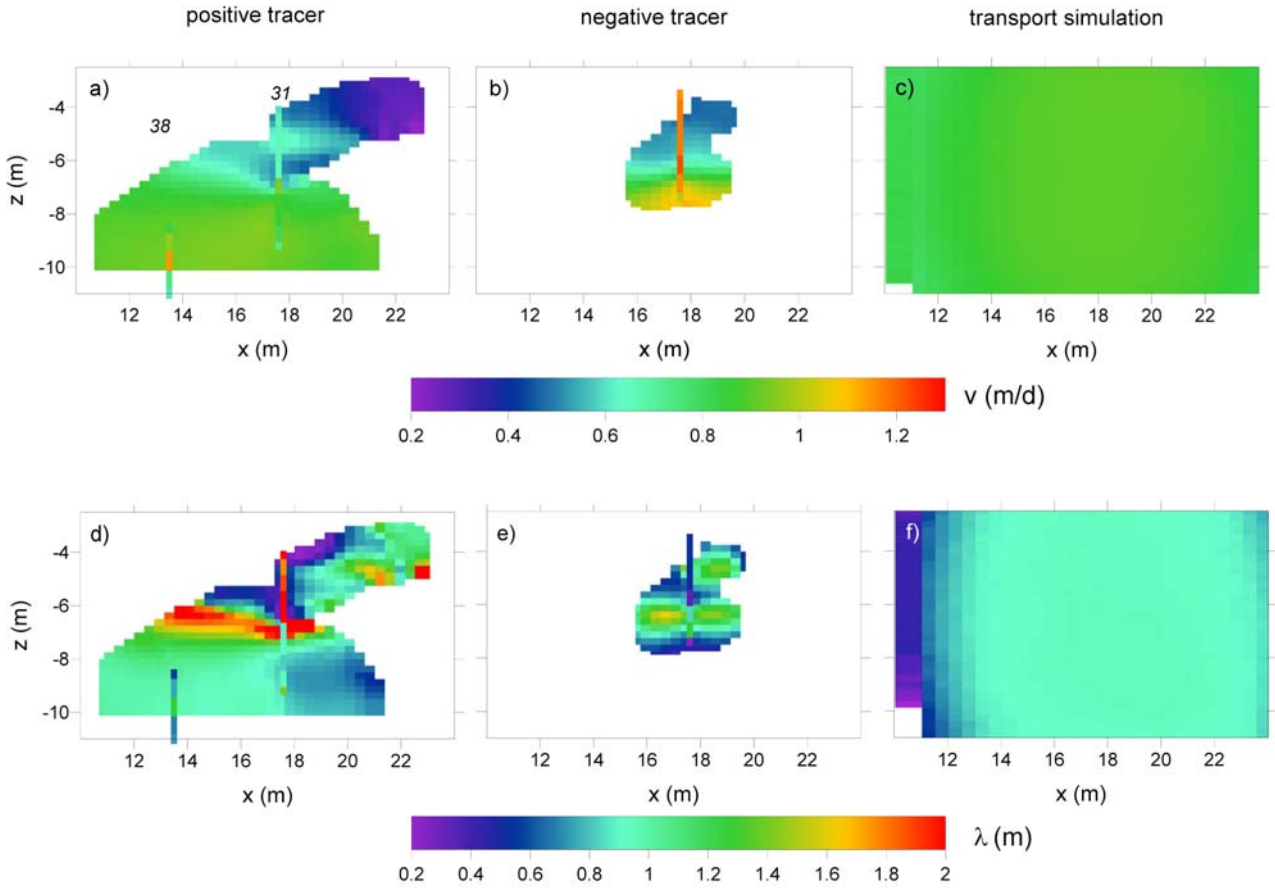

Figure 9. Stream tube (a–c) velocities, v_{eq}, and (d–f) dispersivities, λ_{eq}, in the second ERT image plane for the positive (Figures 9a and 9d) and negative (Figures 9b and 9e) tracer tests and for the transport simulation in a homogeneous aquifer (Figures 9c and 9f). Vertical bars represent stream tube parameters that were derived from breakthrough curves measured with MLS (italic numbers are the well numbers).

in the image planes from fitting equation (9) to time series of relative changes in EC_b. The area in which detectable tracer breakthrough occurred and the average of $C_{0,ERT} - C_{in,ERT}$ in this area are given in Table 3. For comparison, also given in Table 3 is the area through which the flow of water per time unit is equal to the injection rate and the value of $C_{0,ERT} - C_{in,ERT}$ that would be observed when no lateral mixing or dilution would occur between the injection and the image plane and transport would be perfectly one dimensional. The spatial distributions of $C_{0,ERT} - C_{in,ERT}$ in the image planes are shown in Figure 10 for the two tracer experiments and the numerical simulations in the homogeneous aquifer. In order to make a direct comparison between the tracer experiments, the two image planes and the transport simulation, $C_{0,ERT} - C_{in,ERT}$ is normalized with respect to the expected $C_{0,ERT} - C_{in,ERT}$ when transport is one dimensional and no dilution occurs.

[47] The tracer recovery in the first image plane is roughly 50% for both tracer experiments, while this number drops to 20% and 10% in the second image plane for the positive and negative tracer experiments, respectively. Looking at the fitted $C_{0,ERT} - C_{in,ERT}$, the average values in the area where significant breakthrough was observed were close to the expected $C_{0,ERT} - C_{in,ERT}$ when no dilution would occur and transport would be one dimensional, except for the positive tracer experiment and the second image plane. However, the

Table 2. Spatial Averages of Stream Tube Velocities, v_{eq}, and Dispersivities, λ_{eq}[a]

	v_{eq} (m d^{-1})				λ_{eq} (m)			
	First Image Plane		Second Image Plane		First Image Plane		Second Image Plane	
	Positive	Negative	Positive	Negative	Positive	Negative	Positive	Negative
ERT	0.81 (0.24)	0.85 (0.39)	0.75 (0.29)	0.72 (0.30)	1.51 (0.49)	1.04 (1.00)	1.01 (0.38)	0.92 (0.32)
MLS	0.48 (0.40)	0.69 (0.34)	0.78 (0.20)	1.11 (0.07)	1.05 (0.68)	1.44 (0.78)	1.34 (0.58)	0.51 (0.47)
Simulated transport	0.82 (0.03)		0.88 (0.02)		1.02 (0.07)		0.91 (0.03)	

[a]The velocities and dispersivities were obtained from local tracer breakthrough curves in pixels of ERT images, in local multilevel groundwater samplers (MLS) during the positive and negative tracer tests, and in the 3-D flow and transport simulations in a homogeneous aquifer. Values in parentheses are the coefficients of variation of the stream tube parameters within the image plane.

Table 3. Mean Estimated Darcy Flux Through the Image Plane, Relative Changes in Bulk Electrical Conductivity, Areas of Breakthrough, and Recovered Tracer Fraction From Equation (15)

Image Plane	Tracer Test	Mean Estimated Darcy Flux, $\langle q_y \rangle$ (m d^{-1})	$C_{0,ERT} - C_{in,ERT}$ No Dilution[a]	$C_{0,ERT} - C_{in,ERT}$ Fitted[b]	Expected Area of Breakthrough With No Dilution (m^2)	Observed Breakthrough Area (m^2)	Tracer Recovery (%)
First	positive	0.22	4.83	4.54	92	51	51
	negative	0.23	−0.65	−0.88	87	34	53
Second	positive	0.20	4.83	2.32	98	48.	23
	negative	0.19	−0.65	−0.61	103	13	11

[a]Relative changes in bulk electrical conductivity when no dilution would occur.
[b]Average relative changes in bulk electrical conductivity derived from stream tube model fit.

fitted $C_{0,ERT} - C_{in,ERT}$ were locally up to a factor 2 in the first image plane and a factor 1.5 in the second plane larger than the expected ones. Also for the numerical simulations, the fitted $C_{0,ERT} - C_{in,ERT}$ in the central area of the tracer plume breakthrough were up to a factor 1.4 larger in the first and 1.2 in the second image plane than expected for uniform 1-D flow. The simulation results demonstrate that the larger than expected $C_{0,ERT} - C_{in,ERT}$ could be explained by upstream tracer movement during the injection. The observed breakthrough with ERT is focused more in a small area with large $C_{0,ERT} - C_{in,ERT}$ than in the homogeneous aquifer. This could be explained by a larger upstream movement around the injection well in more conductive layers where more tracer solution was injected. The tracer balance calculations indicate that these locally larger $C_{0,ERT} - C_{in,ERT}$ do not entirely compensate for the smaller area in which significant tracer breakthrough is observed with ERT. The length of the plume is expected to be larger in regions with a larger $C_{0,ERT} - C_{in,ERT}$ so that the assumption of an infinitely long tracer plume in the 2.5 D ERT inversion will hold more than in regions where the plume length and $C_{0,ERT} - C_{in,ERT}$ are small. A smaller plume length likely results in smaller changes in measured resistances and may therefore lead to an underestimation of $C_{0,ERT} - C_{in,ERT}$. As a consequence, the 2.5-D inversion may lead to an underestimation of the breakthrough especially at locations where the plume length is small. Based on the breakthrough time and the mean stream tube velocity, the plume length is estimated to be 20 m (assuming a breakthrough time of 20 days (Figure 7) and a stream tube velocity of 1 m d^{-1} (Table 2)). This is similar to the plume length of *Vanderborght et al.* [2005], which is estimated to be 30 m (assuming a breakthrough time of 30 days (*Vanderborght et al.* [2005, Figure 8] and a stream tube velocity of 1 m d^{-1}). The changes in bulk electrical conductivity were larger in the numerical experiment (around 1600 μS cm^{-1} [*Vanderborght et al.* [2005, Figure 4]) than in the current experiments (600 μS cm^{-1} for the positive tracer and −50 μS cm^{-1} for the negative tracer). Finally the width of the tracer plume was considerably larger in the numerical tracer experiment of *Vanderborght et al.* [2005] (50 m) than in the current experiments (10 m). The differences in conductivity contrast and the extension of the plume in the lateral direction may be a cause of the smaller tracer recoveries in the current than in the numerical tracer experiments.

[48] In the positive tracer experiment, the largest $C_{0,ERT} - C_{in,ERT}$ values were observed in the deeper part of the aquifer whereas the opposite holds true for the negative tracer experiment (Figure 10). This suggests that also density driven flow may be a cause for the larger than expected $C_{0,ERT} - C_{in,ERT}$ values. Since ERT-estimated changes in EC_b did not overestimate the changes in EC_b that were derived from the MLS (Figures 5, 6, and 7), the large $C_{0,ERT} - C_{in,ERT}$ cannot be attributed to artifacts resulting from a 2-D approximation of the solute plume in the ERT inversion.

4. Discussion and Conclusion

[49] Two tracer tests were conducted at the Krauthausen test site and were monitored using ERT and multilevel sampling to evaluate the applicability of ERT for characterizing and quantifying subsurface transport processes in a heterogeneous aquifer. The tracer tests were carried out under similar conditions using a positive tracer, with a higher electrical conductivity, and a negative tracer with a lower electrical conductivity than the ambient groundwater. By conducting these two tracer tests, the effect of the tracer on the observed transport could be evaluated. Since, despite the density differences, breakthrough of the two tracers in the image planes overlapped, similarities in breakthrough patterns reflect the effect of aquifer heterogeneity on transport and could be used to evaluate the general repeatability of a tracer test. Laboratory-scale experiments did not show a significant effect of the tracer type on the tracer breakthrough so that geochemical interactions between the tracer solutions and the solid phase did not play an important role in the transport process.

[50] Because a full 3-D characterization of the transport process could not be afforded, we monitored the breakthrough of the tracer plumes at two cross sections downstream of the tracer injection well. The ERT results showed notable differences between the two experiments which can be explained by density driven flow. During the positive tracer experiment, the tracer plume sank down and moved primarily through the lower part of the aquifer whereas the main breakthrough was observed in the middle part of the aquifer during the negative tracer test. The different conductivity contrasts, both in sign and absolute magnitude, in the two tracer experiments lead to different ERT sensitivity and resolution and may explain differences between the ERT observed breakthrough in the two experiments such as the lower mass recovery and smaller area where tracer breakthrough was observed in the negative tracer test.

[51] Aside from these differences, the spatial patterns of the transport processes that were observed with ERT in the two tracer tests showed similar imprints of the aquifer heterogeneity on the transport so that in this respect the tracer test results were quite reproducible. Using ERT, a separation of the solute plume in an upper slower moving part and a

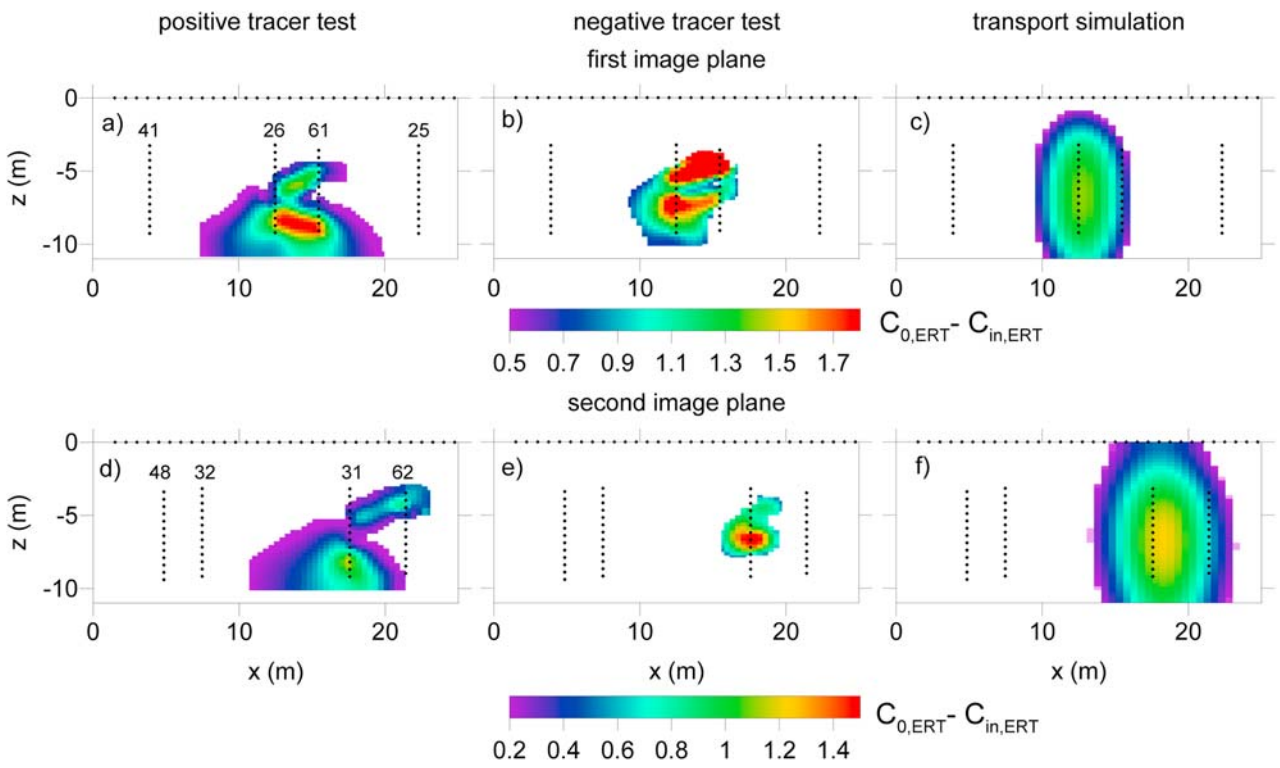

Figure 10. Normalized relative change in bulk electrical, $C_{0,ERT} - C_{in,ERT}$, in the (a–c) first and (d–f) second ERT image plane for the positive (Figures 10a and 10d) and negative (Figures 10b and 10e) tracer tests and for transport simulations in a homogeneous aquifer (Figures 10c and 10f). Electrodes are represented by dots, and numbers in the plots refer to well numbers.

lower faster moving part, which is a signature of the aquifer heterogeneity, could be clearly observed in both image planes and in both experiments.

[52] The comparison between ERT and MLS results showed some agreement in terms of arrival times and peak magnitudes of the tracer breakthrough. However, the observed breakthroughs in the MLS were not very consistent between the two tracer tests. Neither the separation of the tracer plumes in the two image planes and the two experiments nor the effect of density driven flow could be observed in the MLS data. Differences between ERT and MLS derived breakthrough curves may be expected in a heterogeneous flow field due to different sampling volumes of the two methods. But these differences should be similar in the two tracer tests. The inconsistencies in the MLS data rather indicate that the breakthrough observed with MLS may be prone to artifacts. Simultaneous breakthrough that was observed at various depths along a well and a long tailing of high concentrations that was observed at the bottom of the well during the positive tracer experiment could have been caused by a vertical mixing of the tracer solution and a density driven sinking of the tracer within the screened well and the filter gravel. It should be noted that the borehole electrodes were removed after each ERT survey, which may have induced vertical mixing of the tracer solution within the screened well. Since the electrodes need to be in contact with the surrounding aquifer, inflatable silicon hoses to seal the inside of the screened wells could not be installed. Such measures were taken to avoid vertical mixing of tracer solution within the wells in previous tracer studies that were monitored with MLS at the test site [*Vereecken et al.*, 2000]. Several studies have demonstrated the improvement of the ERT results by constraining the inversion with local information [e.g., *Yeh et al.*, 2002]. However, our results indicate that the quality and consistency of the local-scale measurements need to be carefully checked before they can be used to constrain the ERT inversion. Because they are likely more accurate and located in less sensitive regions of the ERT image plane, local measurements with MLS in nonscreened or sealed wells may be more suitable to constrain the ERT inversion than MLS measurements in screened wells in which electrode strings are continuously replaced. However, this requires further investigation.

[53] The spatiotemporal information that was gained with ERT and MLS was interpreted by means of a one-dimensional stream tube model to quantify the observed heterogeneity of the transport processes. Neither the parameters of the petrophysical relationship relating tracer concentration and bulk electrical conductivity nor their spatial distribution in the image plane need to be known, which is an important advantage of using a stream tube model to interpret time sequences of ERT images. The only required assumption is that the petrophysical relationship is linear, which is generally true for hydraulically conductive aquifers with relatively low clay content. Using a stream tube model, the spatiotemporal information that is contained in a set of time frames was effectively condensed in spatial distributions of stream tube parameters. The spatial distribution of the

stream tube velocity clearly contained a signature of the aquifer heterogeneity. The experiments in this study represent upscaled versions of the experiment that was carried out by *Kemna et al.* [2002]. Tracer transport was monitored over a larger travel distance and in a larger cross section of the aquifer, especially also the upper part of the aquifer. As can be expected, this upscaling is reflected in a larger stream tube dispersivity and a larger variation of stream tube velocities. When the cross section of the aquifer in which breakthrough is observed is sufficiently large, the spatial distribution of stream tube velocities could be used to infer the spatial statistics of the hydraulic conductivity in the aquifer [*Vanderborght et al.*, 2005]. However, the lateral extent of the observed tracer plume in this study was too small to obtain a representative image of the aquifer's heterogeneity. Wider tracer plumes could be obtained by injecting tracer solution in a line of wells. Instead of deriving the spatial statistics of the hydraulic conductivity, the ERT data might also be used to infer the spatial distribution of the hydraulic conductivity directly using a so-called coupled hydrogeophysical inversion [*Ferre et al.*, 2009]. In coupled hydrogeophysical inversion, the geophysical measurements are integrated in a flow and transport model inversion. This approach has been demonstrated in numerical experiments for ground penetrating radar data [*Finsterle and Kowalsky*, 2008; *Kowalsky et al.*, 2005; *Linde et al.*, 2006] and for time moments of electrical resistance measurements [*Pollock and Cirpka*, 2008]. To reveal the 3-D structure of the hydraulic conductivity, information about the transport process between the injection well and the image planes is required and, as a consequence, a more extensive 3-D ERT survey than the setup we used here.

[54] Besides the spatial structure of the transport velocity, also the stream tube dispersivity, which is a measure of the dilution of the tracer concentration in the aquifer, can be inferred. Because of numerical mixing associated with the smoothing in the ERT data set inversion, especially in regions with high gradients in stream tube velocity, the ERT-derived stream tube dispersivity may overestimate the real one. The average ERT-derived dispersivities were, however, not consistently larger than the dispersivities that were derived from the MLS data, so that the bias due to numerical mixing is not larger than the uncertainty of MLS-derived dispersivities.

[55] Finally, a tracer balance was calculated for the two image planes from relative changes in bulk electrical conductivity, $C_{0,ERT} - C_{in,ERT}$, an estimate of the water flux, which was derived from the average stream tube velocity and the mean porosity, and an estimate of the average petrophysical parameters, which were derived from lab-scale experiments. The obtained tracer balances ranging from 50% for the first to only 10% for the second image plane, were poor. Similar underestimation of the recovered tracer has been reported in other tracer studies that were monitored with ERT [*Singha and Gorelick*, 2005] and it was there attributed to the smoothing in the ERT inversion in combination with a low signal-to-noise ratio [*LaBrecque et al.*, 1996]. The signal-to-noise ratio clearly decreased from the first to the second image plane. However, the magnitude of the peak electrical conductivity changes that was derived from the ERT results was similar to that observed in the MLS and the fitted $C_{0,ERT} - C_{in,ERT}$ values were at some locations up to a factor two larger than the time-integrated change in bulk electrical conductivity that would be expected for a 1-D transport process. Numerical simulations in a homogeneous aquifer indicated that the large $C_{0,ERT} - C_{in,ERT}$ are partly due to upstream tracer transport during the injection. However, the observed $C_{0,ERT} - C_{in,ERT}$ are locally considerably larger than the simulated ones in a homogeneous aquifer. This indicates that more tracer is injected in layers with a higher conductivity. The tracer recovery could be improved by using apparent petrophysical relations that relate changes in pore fluid conductivity to changes in inverted bulk electrical conductivity [*Singha and Gorelick*, 2006]. Since the ERT sensitivity depends particularly on the spatial distribution of the bulk electrical conductivity, the derivation of such apparent petrophysical relationships must be based on a priori estimations of the tracer migration and the shape of the solute plume. As a consequence, the derived tracer concentrations from ERT results would be based partly on a priori information and partly on the information contained in the ERT measurements. It would be difficult, however, to evaluate which information in the inverted ERT images comes from the a priori information and which comes from ERT data.

[56] As an alternative to the use of apparent petrophysical relations, a tracer recovery constraint could be included in a joint inversion of the ERT data sets of all time frames. We postulate that this would be similar to the use of apparent petrophysical relationships if no a priori information about the location of the tracer breakthrough is available. In a numerical study [*Cassiani et al.*, 2006b], inversion using a tracer recovery constraint resulted in a more or less homogeneous increase of tracer concentrations in the less sensitive regions in the image plane. Since in the present study the peak concentrations were relatively well estimated, at least much better than the total amount of tracer crossing the image plane, and since a tracer recovery constraint primarily leads to an artificial increase of concentrations in low-sensitive regions of the image plane, the only way out seems to be to increase ERT sensitivity using a denser electrode network.

[57] **Acknowledgments.** These tracer experiments were associated with a large logistic effort. Because of safety regulations, the tracer injection, which took place over a period of 7 days, required around-the-clock surveillance by at least two persons. Also, the groundwater sampling campaigns and the electrical conductivity measurements involved the commitment of several people. We would like to acknowledge everyone who assisted us in this experiment. Special thanks are due to Kristina Borgers, Karsten Göβling, Martin Münch, and Arre Verweert, who helped with the ERT measurements and analysis, and to Odillia Esser, Rainer Harms, Anke Langen, and Hans-Günter Sittardt, who helped with the groundwater sampling and electrical conductivity measurements. We would also like to thank the reviewers and the associate editor for their detailed comments on a previous version of this manuscript. J. A. Huisman is supported by grant HU1312/2-1 of the Deutsche Forschungsgemeinschaft.

References

Bellin, A., and Y. Rubin (2004), On the use of peak concentration arrival times for the inference of hydrogeological parameters, *Water Resour. Res.*, *40*, W07401, doi:10.1029/2003WR002179.

Binley, A., S. Henry-Poulter, and B. Shaw (1996), Examination of solute transport in an undisturbed soil column using electrical resistance tomography, *Water Resour. Res.*, *32*(4), 763–769, doi:10.1029/95WR02995.

Binley, A., G. Cassiani, R. Middleton, and P. Winship (2002), Vadose zone flow model parameterisation using cross-borehole radar and resistivity imaging, *J. Hydrol.*, *267*(3–4), 147–159, doi:10.1016/S0022-1694(02)00146-4.

Boggs, J. M., S. C. Young, L. M. Beard, L. W. Gelhar, K. R. Rehfeldt, and E. E. Adams (1992), Field study of dispersion in a heterogeneous aquifer: 1. Overview and site description, *Water Resour. Res.*, *28*(12), 3281–3291, doi:10.1029/92WR01756.

Cassiani, G., V. Bruno, A. Villa, N. Fusi, and A. M. Binley (2006a), A saline trace test monitored via time-lapse surface electrical resistivity tomography, *J. Appl. Geophys.*, *59*(3), 244–259.

Cassiani, G., R. Deiana, and A. Kemna (2006b), Non invasive monitoring of water flow in the vadose zone: The issue of mass balance in controlled tracer injection experiments, *Eos Trans. AGU*, *87*(52), Fall Meet. Suppl., Abstract H44B-01.

Daily, W., A. Ramirez, D. Labrecque, and J. Nitao (1992), Electrical resistivity tomography of vadose water movement, *Water Resour. Res.*, *28*(5), 1429–1442, doi:10.1029/91WR03087.

Day-Lewis, F. D., and K. Singha (2008), Geoelectrical inference of mass transfer parameters using temporal moments, *Water Resour. Res.*, *44*, W05201, doi:10.1029/2007WR006750.

Deiana, R., G. Cassiani, A. Kemna, A. Villa, V. Bruno, and A. Bagliani (2007), An experiment of non-invasive characterization of the vadose zone via water injection and cross-hole time-lapse geophysical monitoring, *Near Surf. Geophys.*, *5*(3), 183–194.

Döring, U. (1997), Transport der reaktiven Stoffe Eosin, Uranin und Lithium in einem heterogenen Grundwasserleiter, Ph.D. thesis, Christian Albrechts Univ., Kiel, Germany.

Englert, A. (2003), Measurement, estimation and modeling of groundwater flow at Krauthausen test site, Ph.D. thesis, RWTH Aachen Univ., Aachen, Germany.

Ferre, T., L. Bentley, A. Binley, N. Linde, A. Kemna, K. Singha, K. Holliger, J. A. Huisman, and B. Minsley (2009), Critical steps for the continuing advancement of hydrogeophysics, *Eos Trans. AGU*, *90*(23), 200, doi:10.1029/2009EO230004.

Finsterle, S., and M. B. Kowalsky (2008), Joint hydrological-geophysical inversion for soil structure identification, *Vadose Zone J.*, *7*(1), 287–293, doi:10.2136/vzj2006.0078.

Franson, M. A. H. (1985), *Standard Methods for the Examination of Water and Waste Water*, 16th ed., Am. Public Health Assoc., Washington, D. C.

French, H., and A. Binley (2004), Snowmelt infiltration: Monitoring temporal and spatial variability using time-lapse electrical resistivity, *J. Hydrol.*, *297*(1–4), 174–186, doi:10.1016/j.jhydrol.2004.04.005.

French, H. K., C. Hardbattle, A. Binley, P. Winship, and L. Jakobsen (2002), Monitoring snowmelt induced unsaturated flow and transport using electrical resistivity tomography, *J. Hydrol.*, *267*(3–4), 273–284, doi:10.1016/S0022-1694(02)00156-7.

Hess, K. M., S. H. Wolf, and M. A. Celia (1992), Large-scale natural gradient tracer test in sand and gravel, Cape Cod, Massachusetts: 3. Hydraulic conductivity variability and calculated macrodispersivities, *Water Resour. Res.*, *28*(8), 2011–2027, doi:10.1029/92WR00668.

Jensen, K. H., K. Bitsch, and P. L. Bjerg (1993), Large-scale dispersion experiments in a sandy aquifer in Denmark: Observed tracer movements and numerical analyses, *Water Resour. Res.*, *29*(3), 673–696, doi:10.1029/92WR02468.

Jury, W. A., and K. Roth (1990), *Transfer Functions and Solute Movement Through Soil: Theory and Application*, Birkhäuser, Basel, Switzerland.

Kachanoski, R. G., E. Pringle, and A. Ward (1992), Field measurement of solute travel-times using time domain reflectometry, *Soil Sci. Soc. Am. J.*, *56*(1), 47–52.

Kemna, A. (2000), Tomographic inversion of complex resistivity: Theory and application, Ph.D. thesis, Ruhr Univ. of Bochum, Bochum, Germany.

Kemna, A., J. Vanderborght, B. Kulessa, and H. Vereecken (2002), Imaging and characterisation of subsurface solute transport using electrical resistivity tomography (ERT) and equivalent transport models, *J. Hydrol.*, *267*(3–4), 125–146, doi:10.1016/S0022-1694(02)00145-2.

Köstel, J. K., A. Kemna, M. Javaux, A. Binley, and H. Vereecken (2008), Quantitative imaging of solute transport in an unsaturated and undisturbed soil monolith with 3-D ERT and TDR, *Water Resour. Res.*, *44*, W12411, doi:10.1029/2007WR006755.

Köstel, J. K., J. Vanderborght, M. Javaux, A. Kemna, A. Binley, and H. Vereecken (2009a), Non-invasive 3D transport characterization in a sandy soil using ERT II: Transport process inference, *Vadose Zone J.*, *8*(3), 723–734, doi:10.2136/vzj2008.0154.

Köstel, J. K., J. Vanderborght, M. Javaux, A. Kemna, A. Binley, and H. Vereecken (2009b), Non-invasive 3D transport characterization in a sandy soil using ERT I: Investigating the validity of ERT-derived transport parameters, *Vadose Zone J.*, *8*(3), 711–722, doi:10.2136/vzj2008.0027.

Kowalsky, M. B., S. Finsterle, J. Peterson, S. Hubbard, Y. Rubin, E. Majer, A. Ward, and G. Gee (2005), Estimation of field-scale soil hydraulic and dielectric parameters through joint inversion of GPR and hydrological data, *Water Resour. Res.*, *41*, W11425, doi:10.1029/2005WR004237.

LaBrecque, D. J., and X. Yang (2001), Difference inversion of ERT data: A fast inversion method for 3-D in situ monitoring, *J. Environ. Eng. Geophys.*, *6*(2), 83–89, doi:10.4133/JEEG6.2.83.

LaBrecque, D. J., M. Miletto, W. Daily, A. Ramirez, and E. Owen (1996), The effects of noise on Occam's inversion of resistivity tomography data, *Geophysics*, *61*(2), 538–548, doi:10.1190/1.1443980.

Leblanc, D. R., S. P. Garabedian, K. M. Hess, L. W. Gelhar, R. D. Quadri, K. G. Stollenwerk, and W. W. Wood (1991), Large-scale natural gradient tracer test in sand and gravel, Cape Cod, Massachusetts: 1. Experimental design and observed tracer movement, *Water Resour. Res.*, *27*(5), 895–910, doi:10.1029/91WR00241.

Linde, N., S. Finsterle, and S. Hubbard (2006), Inversion of tracer test data using tomographic constraints, *Water Resour. Res.*, *42*, W04410, doi:10.1029/2004WR003806.

Looms, M. C., A. Binley, K. H. Jensen, L. Nielsen, and T. M. Hansen (2008a), Identifying unsaturated hydraulic parameters using an integrated data fusion approach on cross-borehole geophysical data, *Vadose Zone J.*, *7*(1), 238–248, doi:10.2136/vzj2007.0087.

Looms, M. C., K. H. Jensen, A. Binley, and L. Nielsen (2008b), Monitoring unsaturated flow and transport using cross-borehole geophysical methods, *Vadose Zone J.*, *7*(1), 227–237, doi:10.2136/vzj2006.0129.

Mallants, D., M. Vanclooster, N. Toride, J. Vanderborght, M. T. van Genuchten, and J. Feyen (1996), Comparison of three methods to calibrate TDR for monitoring solute movement in undisturbed soil, *Soil Sci. Soc. Am. J.*, *60*(3), 747–754.

Michot, D., Y. Benderitter, A. Dorigny, B. Nicoullaud, D. King, and A. Tabbagh (2003), Spatial and temporal monitoring of soil water content with an irrigated corn crop cover using surface electrical resistivity tomography, *Water Resour. Res.*, *39*(5), 1138, doi:10.1029/2002WR001581.

Oldenborger, G. A., M. D. Knoll, P. S. Routh, and D. J. LaBrecque (2007), Time-lapse ERT monitoring of an injection/withdrawal experiment in a shallow unconfined aquifer, *Geophysics*, *72*(4), 177–187, doi:10.1190/1.2734365.

Olsen, P. A., A. Binley, S. Henry-Poulter, and W. Tych (1999), Characterizing solute transport in undisturbed soil cores using electrical and X-ray tomographic methods, *Hydrol. Processes*, *13*(2), 211–221, doi:10.1002/(SICI)1099-1085(19990215)13:2<211::AID-HYP707>3.0.CO;2-P.

Park, S. (1998), Fluid migration in the vadose zone from 3-D inversion of resistivity monitoring data, *Geophysics*, *63*(1), 41–51, doi:10.1190/1.1444326.

Pollock, D., and O. A. Cirpka (2008), Temporal moments in geoelectrical monitoring of salt tracer experiments, *Water Resour. Res.*, *44*, W12416, doi:10.1029/2008WR007014.

Ramirez, A., W. Daily, D. Labrecque, E. Owen, and D. Chesnut (1993), Monitoring an underground steam injection process using electrical resistance tomography, *Water Resour. Res.*, *29*(1), 73–87, doi:10.1029/92WR01608.

Revil, A., and P. W. J. Glover (1998), Nature of surface electrical conductivity in natural sands, sandstones, and clays, *Geophys. Res. Lett.*, *25*(5), 691–694, doi:10.1029/98GL00296.

Rhoades, J. D., N. A. Manteghi, P. J. Shouse, and W. J. Alves (1989), Soil electrical conductivity and soil salinity—New formulations and calibrations, *Soil Sci. Soc. Am. J.*, *53*(2), 433–439.

Singha, K., and S. M. Gorelick (2005), Saline tracer visualized with three-dimensional electrical resistivity tomography: Field-scale spatial moment analysis, *Water Resour. Res.*, *41*, W05023, doi:10.1029/2004WR003460.

Singha, K., and S. M. Gorelick (2006), Hydrogeophysical tracking of three-dimensional tracer migration: The concept and application of apparent petrophysical relations, *Water Resour. Res.*, *42*, W06422, doi:10.1029/2005WR004568.

Singha, K., F. D. Day-Lewis, and J. W. Lane (2007), Geoelectrical evidence of bicontinuum transport in groundwater, *Geophys. Res. Lett.*, *34*, L12401, doi:10.1029/2007GL030019.

Singha, K., A. Pidlisecky, F. D. Day-Lewis, and M. N. Gooseff (2008), Electrical characterization of non-Fickian transport in groundwater and hyporheic systems, *Water Resour. Res.*, *44*, W00D07, doi:10.1029/2008WR007048.

Slater, L., A. Binley, R. Versteeg, G. Cassiani, R. Birken, and S. Sandberg (2002), A 3D ERT study of solute transport in a large experimental tank, *J. Appl. Geophys.*, *49*(4), 211–229, doi:10.1016/S0926-9851(02)00124-6.

Spitzer, K. (1998), The three-dimensional DC sensitivity for surface and subsurface sources, *Geophys. J. Int.*, *134*(3), 736–746, doi:10.1046/j.1365-246x.1998.00592.x.

Sudicky, E. A. (1986), A natural gradient experiment on solute transport in a sand aquifer: Spatial variability of hydraulic conductivity and its role in the dispersion process, *Water Resour. Res.*, *22*(13), 2069–2082, doi:10.1029/WR022i013p02069.

Tillmann, A., A. Englert, Z. Nyari, I. Fejes, J. Vanderborght, and H. Vereecken (2008), Characterization of subsoil heterogeneity, estimation of grain size distribution and hydraulic conductivity at the Krauthausen test site using cone penetration test, *J. Contam. Hydrol.*, *95*(1–2), 57–75, doi:10.1016/j.jconhyd.2007.07.013.

Toride, N., F. J. Leij, and M. T. van Genuchten (1999), The CXTFIT code for estimating transport parameters from laboratory or field tracer experiments, version 2.1, 138 pp., U.S. Salinity Lab., Agric. Res. Serv., U.S. Dep. of Agric., Riverside, Calif.

Vanclooster, M., D. Mallants, J. Diels, and J. Feyen (1993), Determining local-scale solute transport parameters using time-domain reflectometry (TDR), *J. Hydrol.*, *148*(1–4), 93–107, doi:10.1016/0022-1694(93)90254-7.

Vanderborght, J., A. Kemna, H. Hardelauf, and H. Vereecken (2005), Potential of electrical resistivity tomography to infer aquifer transport characteristics from tracer studies: A synthetic case study, *Water Resour. Res.*, *41*, W06013, doi:10.1029/2004WR003774.

Vanderborght, J., R. Kasteel, and H. Vereecken (2006), Stochastic continuum transport equations for field-scale solute transport: Overview of theoretical and experimental results, *Vadose Zone J.*, *5*(1), 184–203, doi:10.2136/vzj2005.0024.

Vereecken, H., U. Döring, H. Hardelauf, U. Jaekel, U. Hashagen, O. Neuendorf, H. Schwarze, and R. Seidemann (2000), Analysis of solute transport in a heterogeneous aquifer: The Krauthausen field experiment, *J. Contam. Hydrol.*, *45*(3–4), 329–358.

Yeh, T. C. J., S. Liu, R. J. Glass, K. Baker, J. R. Brainard, D. Alumbaugh, and D. LaBrecque (2002), A geostatistically based inverse model for electrical resistivity surveys and its applications to vadose zone hydrology, *Water Resour. Res.*, *38*(12), 1278, doi:10.1029/2001WR001204.

Zhou, Q. Y., J. Shimada, and A. Sato (2001), Three-dimensional spatial and temporal monitoring of soil water content using electrical resistivity tomography, *Water Resour. Res.*, *37*(2), 273–285, doi:10.1029/2000WR900284.

A. Englert, Earth Sciences Department, Ruhr-University Bochum, Universitätsstraße 150, D-44801 Bochum, Germany.

J. A. Huisman, J. Rings, J. Vanderborght, and H. Vereecken, Agrosphere Institute, ICG-4, Forschungszentrum Jülich GmbH, D-52425 Jülich, Germany. (j.vanderborght@fz-juelich.de)

A. Kemna, Department of Geodynamics and Geophysics, University of Bonn, Nussallee 8, D-53115 Bonn, Germany.

K. Müller, RWE Dea AG, Überseering 40, D-22297 Hamburg, Germany.